

# Adaptive incomplete multi-view learning via tensor graph completion

Heng Zhang<sup>1</sup> and Xiaohong Chen<sup>\*1</sup>

<sup>1</sup>College of Mathematics, Nanjing University of Aeronautics and Astronautics

August 9, 2022

## Abstract

With the advancement of the data acquisition techniques, multi-view learning has become a hot topic. Some multi-view learning methods assume that the multi-view data is complete, which means that all instances are present, but this too ideal. Certain tensor-based methods for handling incomplete multi-view data have emerged and have achieved better result. However, there are still some problems, such as use of traditional tensor norm which makes the computation high and is not able to handle out-of-sample. To solve these two problems, we proposed a new incomplete multi-view learning method. A new tensor norm is defined to implement graph tensor data recover. The recovered graphs are then regularized to a consistent low-dimensional representation of the samples. In addition, adaptive weights are equipped to each view to adjust the importance of different views. Compared with the existing methods, our method not only explores the consistency among views, but also obtains the low-dimensional representation of the new samples by using the learned projection matrix. An efficient algorithm based on inexact augmented Lagrange multiplier (ALM) method are designed to solve the model and convergence is proved. Experimental results on four datasets show the effectiveness of our method.

**Keywords:** Incomplete multi-view learning, Tensor graph completion,

## 1 Introduction

Multi-view data can provide more information to complete learning tasks compared with the single-view data in many realistic scenarios. Multi-view learning has become an active topic with the large amount of multi-view data being acquired. For different types of learning tasks and data forms, many multi-view learning methods have been proposed, which can be roughly summarized as multi-view transfer learning, multi-view dimension reduction, multi-view clustering, multi-view discriminant analysis, multi-view semi-supervised learning, and multi-view multi-task learning. For a comprehensive review of multi-view learning, please refer to [1]. Most previous methods work well under the assumption that all views of data are complete, i.e., all view representations of each sample are present. However, this assumption usually does not hold due to some instances being missing in practice. For example, in Alzheimer's disease diagnosis [2], the results of all examinations are not available to the subject for various reasons, which leads to incomplete multi-view data. In turn, incomplete multi-view learning has received attention of researchers.

Some incomplete multi-view learning methods have been developed, and the specific ones will be summarized in section 2.1. The graph-based incomplete multi-view learning method has attracted the

---

<sup>\*</sup>lyandcxh@nuaa.edu.cn

attention of many researchers due to the fact that it is a powerful tool for analyzing the relationship among things [3]. Incomplete multi-view spectral clustering with adaptive graph learning (IMSC\_AGL) [4] uses graphs constructed from the low-rank subspace of each view to constrain the consensus low-dimensional representation of each sample. Generalized in complete multi-view clustering with flexible locality structure diffusion (GIMC\_FLSD) [5] introduces graph learning into matrix factorization to obtain unified representation, where the representation preserves the graph information. Incomplete multi-view non-negative representation learning with multiple graphs (IMNRL) [6] performs matrix factorization on multiple incomplete graphs to obtain consensus non-negative representation with graph constraint. Adaptive graph completion based incomplete multi-view clustering (AGC\_IMC) [7] executes consensus representation learning using the self-representation of the graph of each view as regularization on incomplete multi-view data, and further gains the consensus low-dimensional representation. These methods all introduce graph learning to make fuller use of local geometric information among instances, but they only considered the similarity of un-missing instances of intra-view and ignored the similarity of inter-view, which made them unable to explore the complementary information embedded in multiple views well.

In order to explore the high-order correlation information among views, some tensor-based methods are proposed to deal with incomplete multi-view data. Liu et al. [8] used subspace representations with low-rank tensor constraints to explore both the view-specific and cross-view relations among samples and capture the high-order correlations of multiple views simultaneously. Incomplete multi-view tensor spectral clustering with missing view inferring (IMVTSC-MVI) [9] integrates feature space based on missing view inference and manifold space based on similarity graph learning into a unified framework, and introduces low-rank constraint to explore hidden missing view information and to capture high-order correlation information among views. It is worth noting that IMVTSC-MVI treats each view equally, that is, each view has the same weight. Xia et al. [10] obtained a complete graph for each view by taking into account the similarity of graphs among views and using the tensor completion tool, which makes full use of complementary information and spectral structure among views. Although the above tensor-based methods have achieved good performance, there are still some problems. Most of the existing work is to impose a low-rank constraint on the rotated graph tensor, which greatly increased the computational cost. This is because performing SVD on each transverse slice of the rotated tensor of  $n \times m \times n$  is usually very time-consuming, where  $n$  and  $m$  are the number of samples and views respectively. To this end, a tensor nuclear norm based on semi-orthogonal matrix is redefined to reduce computation in this paper.

Specifically, our method is named adaptive incomplete multi-view learning via tensor graph completion (AIML\_TGC), which integrates tensor graph completion, adaptive weight, and consistent subspace learning into a unified framework. Different above work, we redefine a tensor nuclear norm based on a semi-orthogonal matrix in order to reduce the computation of the solution and provide a shrinkage operator to obtain the analytical solution of the subproblem. AIML\_TGC has the unique advantage of subspace, that is, it can process out-of-samples to obtain its low-dimensional representation. To sum up, the contributions of this paper are summarized as follows:

1. An incomplete multi-view learning method based on a tensor completion technique is proposed. Different from the existing multi-view learning method based on tensor norm, we redefine the tensor nuclear norm based on semi-orthogonal to reduce computational cost and assigned weights to each view adaptively.
2. A shrinkage operator is provided to obtain a analytical solution to the subproblem with redefined nuclear norm. The solution method based on the inexact augmented Lagrange multiplier (ALM) is proposed, and its convergence is proved under mild conditions.
3. Extensive experiments show that this method is effective in clustering tasks on four datasets.

The structure of this paper is outlined as follows: Section 2 introduces related work briefly. Section 3 proposes our incomplete multi-view learning method (AIML\_TGC), and gives the solving process in detail. Section 4 verifies the effectiveness of the proposed method through a series of numerical experiments. Section 5 summarizes the whole paper.

## 2 Preliminaries and Related Work

In this section, we summarize some of the notations and basic definitions that will be used in this paper, as well as relevant literature on processing incomplete multi-view data in recent years.

### 2.1 Related Work

A large number of related work has evolved rapidly in the past few years. In this section, incomplete multi-view learning approaches and the use of tensor in multi-view learning will be briefly summarized.

We classify incomplete multi-view learning methods into five categories, i.e. subspace learning based methods, non-negative matrix factorization based methods, graph learning methods, deep neural network based methods, and probabilistic perspective based method. Each category is specified below.

1. Subspace learning based methods [11][12][13][14][15][16]: These methods project all existing views into a common low-dimensional subspace and align all views in this subspace to obtain a consistent low-dimension representation. For example, Yang et al. [15] used sparse low-rank subspace representation to jointly measure relationships intraview relations and interview relations, and then proposed an incomplete multi-view dimension reduction method. Chen et al. [12] proposed semi-paired and semi-supervised generalized correlation analysis (S<sup>2</sup>GCA) based on canonical correlation analysis (CCA), which not only processes incomplete data, but also is applicable to semi-supervised scenario.
2. Non-negative matrix factorization (NMF) based methods [17][18][19][20][21][5][22][6]: These methods aim to decompose the data matrix of each view into the product of the corresponding view's basis matrix and common representation matrix, and then proceed with the next step based on the representation matrix. For example, Li et al. [17] proposed NMF based partial multi-view clustering to learn a common representation for complete samples and private latent representation with the same basis matrix. Multi-view learning with incomplete views (MVL-IV) [18] factorizes the incomplete data matrix of each view as the product of a common representation matrix and corresponding view's basis matrix with low-rank property.
3. Graph learning based methods [23][7][4][24][25][26][27][28]: These methods use the consensus among views to construct graph matrix (or kernel matrix) so that the geometry structure can be preserved, which mainly includes spectral clustering and multi-kernel learning. For example, adaptive graph completion based incomplete multi-view clustering (AGC-IMC) [7] obtains common graph by introducing the self-representation regularization term of the graph matrix, and further gains the consensus low-dimensional representation of the samples. Incomplete multiple kernel k-means with mutual kernel completion (MKKM-IK-MKC) [23] adaptively imputes incomplete kernel matrices, and combines imputation and clustering to achieve higher clustering performance.
4. Deep neural network based methods [29][30][31][32][33]: These methods make use of neural network's powerful learning ability to obtain deeper and complete feature representation. For example, Zhao et al. [30] developed a novel incomplete multi-view clustering method, which projects all multi-view data to a complete and unified representation with the constrain of intrinsic geometric structure. Wang et al. [32] and Xu et al. [33] proposed incomplete multi-view clustering methods based on generative adversarial network (GAN) [34], aiming at two-view and multi-view data respectively, i.e., they use existing views to generate missing views. Lin et al. [35] introduced the ideal of contrast prediction from self-supervised learning in to incomplete multi-view learning to explore the consensus between views by maximizing mutual information and minimizing conditional entropy.
5. Probabilistic perspective based methods [36][37][38][39]: These methods usually use Bayesian statistics, Gaussian models, Variational inference, and other tools to model multi-view data from a probabilistic perspective. For example, Li et al. [38] used shared gaussian process latent variable model

to model the incomplete multi-view data for clustering. Matsuura et al. proposed generalized bayesian canonical correlation analysis with missing modalities (GBCCA-M2) [37] by combining Bayesian CCA [40] and Semi-CCA [41] to process incomplete multi-view data with high dimension.

There are two ways to use tensor in the field of multi-view learning. One way is to look at multi-view data as higher order data and process them by some higher order data methods. The other is to use the method of processing tensor to capture the higher information among views. A representative approach in the first way is tensor canonical correlation analysis (TCCA) [42]. TCCA defines a covariance tensor to handle multi-view data with arbitrary number of views by extending the mutual covariance matrix in canonical correlation analysis (CCA). Deep TCCA (DTCCA) [43] is further proposed by combining it with deep learning. Unlike kernel TCCA, DTCCA can not only handle multi-view data with arbitrary number of views in a nonlinear manner, but also does not need to maintain the train data for computing representations of any given data, which means that a large amount of data can be handled. Cheng et al. [44] viewed the multi-view data as a 3-order tensor and constructed the self-representation tensor by reconstructing the coefficients. Further the Tucker decomposition is used to obtain a low-dimensional representation of samples. The second way usually assumes that the graphs or representation weight matrices of different view are similar, and thus the tensor composed of them is assumed to be of low rank. Low-rank Tensor constrained Multiview Subspace Clustering (LT-MSC) [45] regards the subspace representation matrices of different views as a tensor to capture the higher-order consensus information among views. And this tensor is equipped with low-rank constraints to reduce the redundancy of the learned subspaces and improve the clustering performance. Wu et al. [46] combined the ideal of robust principle component analysis using tensor singular value decomposition based tensor nuclear norm to preserve the low-rankness of a tensor constructed based on a multi-view transition probability matrices of the Markov chain. Kernel  $k$ -means coupled graph tensor (KCGT) [47] uses kernel matrices to construct graph with symmetry and properties of block diagonal. Further these graphs are stacked into a low-rank graph tensor for capturing the high order affinity of all these graphs.

## 2.2 Preliminaries

Tensor and matrices are denoted by uppercase calligraphic letters and italic capital letters respectively, e.g.  $\mathcal{X} \in \mathbb{R}^{n_1 \times n_2 \times n_3}$  and  $X \in \mathbb{R}^{n_1 \times n_2}$ . We denote  $\mathcal{X}_{(i,j,k)}$  and  $X_{(i,j)}$  are  $i, j, k$ -th element of  $\mathcal{X}$  and  $i, j$ -th element of  $X$  respectively. Some basic definitions of tensor are shown below.

Table 2.1: Some notations and descriptions used in this article.

Notations	Descriptions
$\mathcal{X}_{(i,j,k)}$	The $i, j, k$ -th element of the tensor $\mathcal{X}$ .
$X_{(i,j)}$	The $i, j$ -th element of the matrix $X$ .
$\mathcal{X}_{(:, :, i)}$ or $X^{(i)}$	The $i$ -th frontal slice of the tensor $\mathcal{X}$ .
$X_{(:, i)}$	The $i$ -th column of the matrix $X$ .
$X^\top$	The transpose of the matrix $X$ .
$\ X\ _*$	The nuclear norm of the matrix $X$ .
$\ X\ _F$	The Frobenius norm of the matrix $X$ .
$\ \mathcal{X}\ _F$	The Frobenius norm of the tensor $\mathcal{X}$ , i.e. $\sqrt{\sum_{i,j,k} \mathcal{X}_{(i,j,k)}^2}$ .
$\sigma_i(X)$	The $i$ -th smallest singular value of the matrix $X$ .
$\langle \mathcal{X}, \mathcal{Y} \rangle$	The inner product of the tensor $\mathcal{X}$ and $\mathcal{Y}$ , i.e. $\sum_{i,j,k} \mathcal{X}_{(i,j,k)} \mathcal{Y}_{(i,j,k)}$ .
$\nabla f(x)$	The gradient of the function $f(x)$ .
$x_i$	The $i$ -th element of the vector $x$ .

**Definition 2.1** (*unfold* and *fold*). For a 3-order tensor  $\mathcal{X} \in \mathbb{R}^{n_1 \times n_2 \times n_3}$ , we have

$$\text{unfold}(\mathcal{X}) = \begin{bmatrix} X^{(1)} \\ X^{(2)} \\ \vdots \\ X^{(n_3)} \end{bmatrix} = \left[ X^{(1)}; X^{(2)}; \dots; X^{(n_3)} \right] \in \mathbb{R}^{n_1 n_3 \times n_2}, \quad (1)$$

$$\text{fold}(\text{unfold}(\mathcal{X})) = \mathcal{X}. \quad (2)$$

**Definition 2.2** (transformed tensor of  $\mathcal{X}$ ). For a 3-order tensor  $\mathcal{X} \in \mathbb{R}^{n_1 \times n_2 \times n_3}$ , given an matrix  $\Phi \in \mathbb{R}^{n_3 \times n_3}$ , the transformed tensor of the tensor  $\mathcal{X}$  is defined as

$$\mathcal{X}_\Phi = \text{fold} \left( \begin{bmatrix} \mathcal{X}_{(:,1,:)} \\ \mathcal{X}_{(:,2,:)} \\ \vdots \\ \mathcal{X}_{(:,n_1,:)} \end{bmatrix} \Phi \right) \in \mathbb{R}^{n_1 \times n_2 \times n_3}. \quad (3)$$

**Definition 2.3** ( $\Phi$ -Transformed Tensor Nuclear Norm,  $\Phi$ -TTNN). For a 3-order tensor  $\mathcal{X} \in \mathbb{R}^{n_1 \times n_2 \times n_3}$ , given an orthogonal matrix  $\Phi \in \mathbb{R}^{n_3 \times n_3}$ , the  $\Phi$ -TTNN of the tensor  $\mathcal{X}$  is defined as

$$\|\mathcal{X}\|_{\Phi\text{-TTNN}} = \sum_{i=1}^{n_3} \|X_{\Phi}^{(i)}\|_*. \quad (4)$$

## 3 Proposed Method

### 3.1 The proposed model

CCA is classical and effective method for learning multiple view, where the goal is to find two projection vector for two views in order to maximize the correlation between the two projected views. Note that CCA can handle data from only two views, for this reason generalized CCA (GCCA) [48] is proposed to handle data from multiple views. Specifically, given a multi-view dataset  $\{X_i \in \mathbb{R}^{d_i \times n}\}_{i=1}^m$ , the model of GCCA is as follows,

$$\begin{aligned} \min_{A, \{W_i\}_{i=1}^m} \quad & \sum_{i=1}^m \|A - W_i^\top X_i\|_F^2 \\ \text{s.t.} \quad & AA^\top = I \end{aligned} \quad (5)$$

Symbol  $A$  and  $\{W_i\}_{i=1}^m$  in Eq.(5) are the consistent low-dimensional representation matrix of the samples and the projection matrix of each view, respectively. The geometric structure among samples is a valid priori information for the subsequent tasks. As mentioned in the introduction, graph can be exploring the relationship between things. For this reason, graph multi-view CCA (GMCCA) [49] is proposed to obtain consistent low-dimensional representation with structure preservation, and its objective function is

$$\begin{aligned} \min_{A, \{W_i\}_{i=1}^m} \quad & \sum_{i=1}^m \|A - W_i^\top X_i\|_F^2 + \lambda \text{tr}(AL_G A^\top) \\ \text{s.t.} \quad & AA^\top = I \end{aligned} \quad (6)$$

where  $L_G$  is the preconstructed graph Laplacian matrix and  $\lambda$  is the regularization parameter.

A model capable of handing incomplete multi-view data is designed based on Eq.(6) and combined with tensor recover in this paper. For a given incomplete multi-view dataset with  $m$  views and  $n$  samples  $\{X_i \in \mathbb{R}^{d_i \times n}\}_{i=1}^m$ , whose missing instance filled by  $\mathbf{0}$  (i.e. if  $j$ -th instance of  $i$ -th view is missing, then  $X_{i(:,j)} = \mathbf{0}$ ) and the missing information of each view are recorded in a diagonal matrix  $\{P_i \in \mathbb{R}^{n \times n}\}_{i=1}^m$ .  $P_i$  is defined as follows,

$$P_{i(j,j)} = \begin{cases} 1 & \text{if } j\text{-th instance of the } i\text{-th view is not missing} \\ 0 & \text{otherwise} \end{cases}.$$

Symbol  $d_i$  is feature dimension of the  $i$ -th view. Denote  $n_i$  as the number of available instance of the  $i$ -th. Based on Eq.(6), a naive model for handing incomplete multi-view data is designed as follows,

$$\begin{aligned} \min_{A, \{W_i\}_{i=1}^m} \quad & \sum_{i=1}^m \left( \| (A - W_i^\top X_i) P_i \|_F^2 + \lambda \operatorname{tr} (A L_{G_i} A^\top) \right) \\ \text{s.t.} \quad & A A^\top = I \end{aligned} \quad (7)$$

where  $L_{G_i}$  is the Laplacian matrix of preconstructed graph  $G_i$  of the  $i$ -th view. It is worth noting that model (7) treats each view equally, which is usually unrealistic. For this reason, inspired by Nie et al. [50], weight  $\bar{\delta}_i$  are introduced to distinguish the importance of different views as follows,

$$\bar{\delta}_i = \frac{1}{\sqrt{\| (A - W_i^\top X_i) P_i \|_F^2 + \lambda \operatorname{tr} (A L_{G_i} A^\top)}}. \quad (8)$$

Intuitively, if  $i$ -th view is good, then  $\| (A - W_i^\top X_i) P_i \|_F^2$  and  $\operatorname{tr} (A L_{G_i} A^\top)$  should be small, and thus the weight  $\bar{\delta}_i$  for  $i$ -th view is large accordingly Eq.(8). However, it is worth noting that if a view has a high missing rate, it will also make the weight that view larger. To avoid this phenomenon we improve the weight to  $\delta_i = n_i \bar{\delta}_i$ .

Unfortunately, it is not possible to directly construct a complete graph for each view due to the incompleteness of incomplete multi-view data. Therefore,  $G_i$  needs to be completed. Consistency among views is an important property of multi-view data. The graphs among different views should be highly similar in response to consistency among views. Drawing inspiration from the filed of tensor recovery, the objective function for graph recovery is as follows,

$$\begin{aligned} \min_{\mathcal{G}} \quad & \|\mathcal{G}\|_{\Phi, w, S_p}^p + \frac{\gamma}{2} \|P_w(\mathcal{G}) - P_w(\mathcal{M})\|_F^2 \\ \text{s.t.} \quad & G_i \geq 0, \quad G_i \mathbf{1} = \mathbf{1} \end{aligned} \quad (9)$$

where  $\mathcal{G} \in \mathbb{R}^{n \times m \times n}$  and  $\mathcal{G}_{(:,i,:)} = G_i$ .  $\mathcal{M} \in \mathbb{R}^{n \times m \times n}$  is the preconstructed incomplete graph tensor with missing positions filled by 0, where  $\mathcal{M}_{(:,i,:)} = M_i$  is the preconstructed graph of the  $i$ -th view.  $P_w(\cdot)$  is the orthogonal projection onto the liner subspace of tensors supported on  $w = \{(i, j, k) | \mathcal{M}_{(i,j,k)} \text{ is not missing}\}$ :  $P_w(\mathcal{M})_{(i,j,k)} = \mathcal{M}_{(i,j,k)}$  if  $(i, j, k) \in w$  and  $P_w(\mathcal{M})_{(i,j,k)} = 0$  otherwise.  $\|\cdot\|_{\Phi, w, S_p}$  is redefined tensor norm as follows,

**Definition 3.1** ( $\Phi$ -Transformed weight Schatten- $p$  Tensor Nuclear Norm). Given tensor  $\mathcal{X} \in \mathbb{R}^{n_1 \times n_2 \times n_3}$ ,  $h = \min(n_1, n_3)$ , weight vector  $w \in \mathbb{R}^h$  with  $w_1 \geq w_2 \geq \dots \geq w_l \geq 0$ ,  $0 < p \leq 1$ , and transformed matrix  $\Phi \in \mathbb{R}^{n_3 \times r}$ , then

$$\|\mathcal{X}\|_{\Phi, w, S_p} = \left( \sum_{i=1}^{n_3} \|X_\Phi^{(i)}\|_{w, S_p}^p \right)^{\frac{1}{p}} = \left( \sum_{i=1}^{n_3} \sum_{j=1}^h w_j \sigma_j \left( X_\Phi^{(i)} \right)^p \right)^{\frac{1}{p}}. \quad (10)$$

*Remark 3.1.* Note that in some previous literature, the transform matrix is usually an orthogonal square matrix, i.e.,  $\Phi^\top \Phi = I$  and  $r = n_3$ . Our empirical study shows that this is not necessary. Therefore, a semi-orthogonal matrix is used as the transform matrix in this paper, i.e.,  $\Phi^\top \Phi = I$  and  $r < n_3$ . This will reduce the computational effort, i.e.,  $n_3$  singular value decomposition were required, but now only  $r$  are needed. The experimental study in section 4.5 shows that  $r = n_3$  may not be optimal.

Combining the graph recovery model (9) with Eq.(7) and introducing weights  $\{\delta_i\}_{i=1}^m$  gives our proposed method as follow,

$$\begin{aligned} \min_{A, \{W_i\}_{i=1}^m, \mathcal{G}} \quad & \sum_{i=1}^m n_i \sqrt{\left\| (A - W_i^\top X_i) P_i \right\|_F^2 + \lambda \operatorname{tr}(A L_{G_i} A^\top) + \mu \|\mathcal{G}\|_{\Phi, w, S_p}^p + \frac{\gamma}{2} \|P_w(\mathcal{G}) - P_w(\mathcal{M})\|_F^2}, \\ \text{s.t.} \quad & A A^\top = I, \quad G_i \geq 0, \quad G_i \mathbf{1} = \mathbf{1} \end{aligned} \quad (11)$$

where  $\mu > 0$  is the regularization parameter. The pipeline of the proposed method is plotted in Fig.3.1.

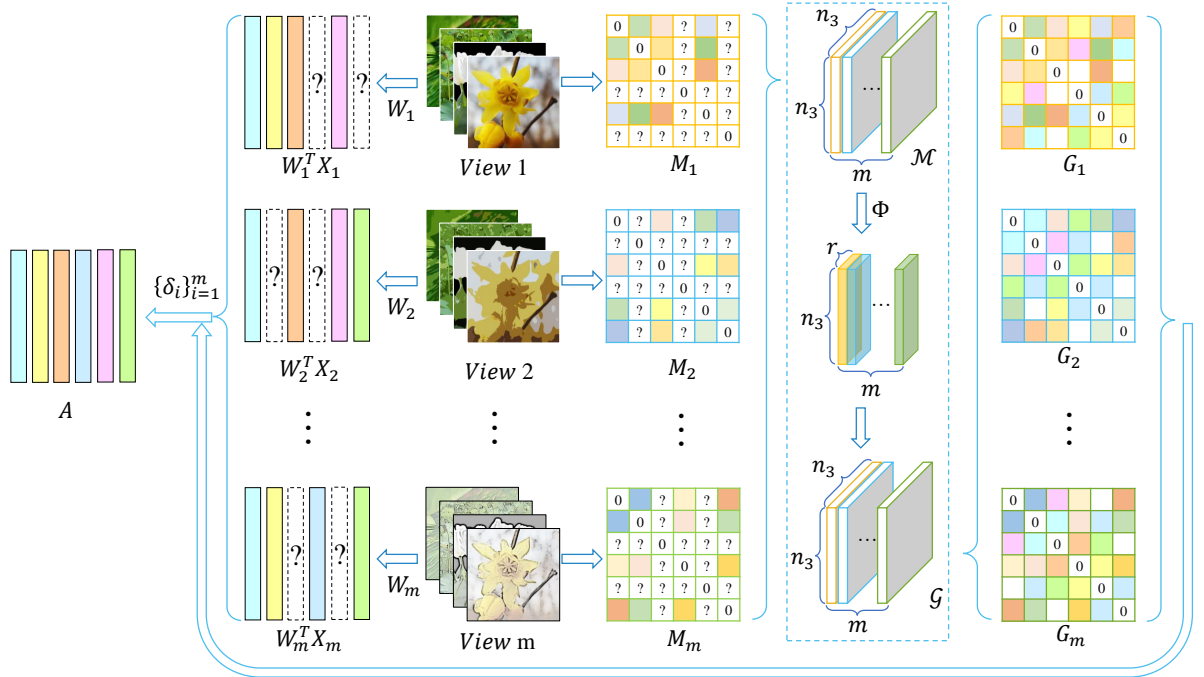


Figure 3.1: The framework of the proposed method.

*Remark 3.2.* Lemma 1 shows that the number of zero eigenvalues of the Laplacian matrix  $L_G$  should be constrained to  $c$  if a graph  $G$  with  $c$  number of connected components is obtained. That is,  $\sum_{i=1}^c \sigma_i(L_G)$  should equal zeros. According to Ky Fan's theory [51], the following equation holds,

$$\sum_{i=1}^c \sigma_i(L_G) = \min_{F F^\top = I, F \in \mathbb{R}^{c \times n}} \operatorname{tr}(F L_G F^\top). \quad (12)$$

This is consistent with the second term in Eq.(11), which implies that our method can be learned a consistent low-dimensional representation that is more conducive to clustering. It is worth noting that the presence of the first term of Eq.(11) allows our method to handle out-of-sample.

**Lemma 1.** [52] *The number of zero eigenvalues of Laplacian matrix  $L_G$  is equal to the number of connected components of the graph  $G$ .*

### 3.2 Solution

To efficiently solve our challenging problem (11), we need to introduce the auxiliary variable  $\mathcal{Y}$  to split the interdependent term such that they can be solved independently. Thus we can reformulate problem (11) into the following equivalent form,

$$\begin{aligned} \min_{A, \{W_i\}_{i=1}^m, \mathcal{G}} \quad & \sum_{i=1}^m \left( \delta_i \left\| \left( A - W_i^\top X_i \right) P_i \right\|_F^2 + \lambda \delta_i \operatorname{tr} (A L_{G_i} A^\top) \right) + \mu \|\mathcal{Y}\|_{\Phi, w, S_p}^p + \frac{\gamma}{2} \|P_w(\mathcal{G}) - P_w(\mathcal{M})\|_F^2 \\ \text{s. t.} \quad & A A^\top = I, \quad G_i \geq 0, \quad G_i \mathbf{1} = \mathbf{1}, \quad \mathcal{G} = \mathcal{Y}, \quad \delta_i = \frac{n_i}{\sqrt{\left\| \left( A - W_i^\top X_i \right) P_i \right\|_F^2 + \lambda \operatorname{tr} (A L_{G_i} A^\top)}} \end{aligned} \quad (13)$$

Inspired by recent progress on alternating direction methods, we proposed efficient algorithm based on inexact augmented Lagrange multiplier (ALM) method to solve the problem (13), whose augmented Lagrangian function is given by

$$\begin{aligned} L_\rho(A, \{W_i\}_{i=1}^m, \mathcal{G}, \mathcal{Y}, \mathcal{C}) = & \sum_{i=1}^m \left[ \delta_i \left\| \left( A - W_i^\top X_i \right) P_i \right\|_F^2 + \lambda \delta_i \operatorname{tr} (A L_{G_i} A^\top) \right] + \mu \|\mathcal{Y}\|_{\Phi, w, S_p}^p \\ & + \frac{\gamma}{2} \|P_w(\mathcal{G}) - P_w(\mathcal{M})\|_F^2 + \langle \mathcal{C}, \mathcal{G} - \mathcal{Y} \rangle + \frac{\rho}{2} \|\mathcal{G} - \mathcal{Y}\|_F^2 \end{aligned} \quad (14)$$

where  $\rho > 0$  is the penalty parameter,  $\mathcal{C} \in \mathbb{R}^{n \times m \times n}$  is Lagrange multipliers. This section uses superscripts to indicate the number of iterations, i.e.  $A^k$  or  $A^{k+1}$ , etc.

#### 3.2.1 Updating $A^{k+1}$ and $\{W_i^k + 1\}_{i=1}^m$

To update  $A^{k+1}$  and  $\{W_i^{k+1}\}_{i=1}^m$ , we consider the following optimization problems,

$$\begin{aligned} A^{k+1}, \{W_i^{k+1}\}_{i=1}^m = & \arg \min_{A, \{W_i\}_{i=1}^m} \sum_{i=1}^m \left( \delta_i^k \left\| \left( A - W_i^\top X_i \right) P_i \right\|_F^2 + \lambda \delta_i^k \operatorname{tr} (A L_{G_i^k} A^\top) \right) \\ \text{s. t.} \quad & A A^\top = I \end{aligned} \quad (15)$$

After simple algebraic operations, problem (15) can be transformed into the following eigenvalue problem,

$$\left( \sum_{i=1}^m \delta_i^k \left( P_i - P_i X_i^\top (X_i P_i X_i^\top)^{-1} X_i P_i + \lambda L_{G_i^k} \right) \right) A^\top = A^\top \Sigma, \quad (16)$$

where  $\Sigma$  is a diagonal matrix of eigenvalues. Then  $A^\top$  can be obtained from the eigenvector corresponding to the first  $d$  largest eigenvalues, where  $d$  is the dimension of consistent low-dimensional representation (i.e.  $A \in \mathbb{R}^{d \times n}$ ). With the  $A$ , we can obtain  $W_i^{k+1} = (X_i P_i X_i^\top)^{-1} X_i P_i A^{k+1 \top}$  for  $i = 1, 2, \dots, m$ . Once  $A^{k+1}$  and  $\{W_i^{k+1}\}_{i=1}^m$  are obtained, the  $\{\delta_i\}_{i=1}^m$  can be updated according to the definition to obtain  $\{\delta_i^{k+1}\}_{i=1}^m$ .



### 3.2.2 Updating $\mathcal{G}^{k+1}$

To solve  $\mathcal{G}^{k+1}$ , we fix the other variable and solve the following optimization problem,

$$\begin{aligned} \mathcal{G}^{k+1} = \arg \min_{\mathcal{G}} \quad & \lambda \sum_{i=1}^m \delta_i^{k+1} \text{tr} \left( A^{k+1} L_{G_i} A^{k+1 \top} \right) + \frac{\gamma}{2} \|P_w(\mathcal{G}) - P_w(\mathcal{M})\|_F^2 + \frac{\rho^k}{2} \left\| \mathcal{G} - \mathcal{Y}^k + \frac{\mathcal{C}^k}{\rho^k} \right\|_F^2 \\ \text{s. t.} \quad & G_i \geq 0, \quad G_i \mathbf{1} = \mathbf{1} \end{aligned} \quad (17)$$

Problem (17) is a least squares problem with constrains. Notice that each tube of the tensor of problem (17) is independent, so it can be converted into  $n \times m$  independent subproblems. Without loss of generality, we let  $g \in \mathbb{R}^{n_3}$ ,  $s \in \mathbb{R}^{n_3}$ ,  $y \in \mathbb{R}^{n_3}$ ,  $\omega \in \mathbb{R}^{n_3}$ ,  $c \in \mathbb{R}^{n_3}$ , and  $t \in \mathbb{R}^{n_3}$  be some tubes of tensor  $\mathcal{G}$ ,  $\mathcal{M}$ ,  $\mathcal{Y}$ ,  $w$ ,  $\mathcal{C}$ , and  $\mathcal{T}$ , respectively, where  $\mathcal{T}_{(i,j,l)}^k = \frac{1}{2} \lambda \delta_l^{k+1} \left\| A_{(:,i)}^{k+1} - A_{(:,j)}^{k+1} \right\|_F^2$ . Thus the following optimization problem can be obtained,

$$\begin{aligned} g^{k+1} = \arg \min_g \quad & \frac{1}{\rho^k} t^k \top g + \frac{\gamma}{2\rho^k} \|P_\omega(g) - P_\omega(z)\|_F^2 + \frac{1}{2} \left\| g - y^k + \frac{c^k}{\rho^k} \right\|_F^2 \\ \text{s. t.} \quad & g \geq 0, \quad \mathbf{1}^\top g = 1 \end{aligned} \quad (18)$$

The Lagrangian function of Eq.(18) is

$$L(g, \alpha, \beta) = \frac{1}{\rho^k} t^k \top g + \frac{\gamma}{2\rho^k} \|P_\omega(g) - P_\omega(z)\|_F^2 + \frac{1}{2} \left\| g - y^k + \frac{c^k}{\rho^k} \right\|_F^2 - \alpha (\mathbf{1}^\top g - 1) - \beta^\top g. \quad (19)$$

where  $\alpha \in \mathbb{R}$  and  $\beta \in \mathbb{R}^{n_3}$  are multipliers. Taking the derivative w.r.t.  $g$  and setting it to zero, the following equation holds,

$$g - y^k + \frac{c^k}{\rho^k} + \frac{\gamma}{\rho^k} (P_\omega(g) - P_\omega(z)) + \frac{1}{\rho^k} t^k - \alpha \mathbf{1} - \beta = \mathbf{0}. \quad (20)$$

The according to the KKT condition, i.e.,  $\mathbf{1}^\top g = 1$ , we have

$$\alpha = \frac{1}{n} \left( 1 - \mathbf{1}^\top y^k + \mathbf{1}^\top \frac{c^k}{\rho^k} + \frac{\gamma}{\rho^k} \mathbf{1}^\top (P_\omega(g) - P_\omega(z)) + \frac{1}{\rho^k} \mathbf{1}^\top t^k - \mathbf{1}^\top \beta \right). \quad (21)$$

Combining Eq.(20) and Eq.(21), we can obtain

$$\begin{aligned} g + \frac{\gamma}{\rho^k} P_\omega(g) = & y^k - \frac{c^k}{\rho^k} + \frac{\gamma}{\rho^k} P_\omega(z) - \frac{1}{\rho^k} t^k - \frac{1}{n} \mathbf{1} \mathbf{1}^\top \left( y^k - \frac{c^k}{\rho^k} + \frac{\gamma}{\rho^k} P_\omega(z) - \frac{1}{\rho^k} t^k \right) + \frac{1}{n} \mathbf{1} \\ & + \frac{1}{n} \mathbf{1} \mathbf{1}^\top \left( \frac{\gamma}{\rho^k} P_\omega(g) - \beta \right) + \beta \end{aligned} \quad (22)$$

Further according to the complementary relaxation in the KKT condition, we have

$$g_i^{k+1} + \frac{\gamma}{\rho^k} P_\omega(g^{k+1})_i = \left( u_i^k - \frac{1}{n} \mathbf{1}^\top u^k + \frac{1}{n} + v^k \right)_+ \quad (23)$$

where  $u^k = y^k - \frac{c^k}{\rho^k} + \frac{\gamma}{\rho^k} P_\omega(z) - \frac{1}{\rho^k} t^k$ ,  $v^k = \frac{1}{n} \mathbf{1}^\top \left( \frac{\gamma}{\rho^k} P_\omega(g^{k+1}) - \beta \right)$ . So we can get

$$g_i^{k+1} = \begin{cases} \left( u_i^k - \frac{1}{n} \mathbf{1}^\top u^k + \frac{1}{n} + v^k \right)_+, & \text{if } i \in \omega, \\ \frac{\rho^k}{\rho^k + \gamma} \left( u_i^k - \frac{1}{n} \mathbf{1}^\top u^k + \frac{1}{n} + v^k \right)_+, & \text{otherwise.} \end{cases} \quad (24)$$

Since  $\mathbf{1}^\top g^{k+1} = 1$ , the value of  $v^k$  can be found by solving the roots of the following function.

$$f(v) = \sum_{i=1}^n g_i^{k+1} - 1 \quad (25)$$

Equation (25) can be solved by Newton's method. The first order derivative of  $f(v)$  is

$$\nabla f(v) = \sum_{i=1}^n \nabla g_i^{k+1}, \quad (26)$$

where

$$\nabla g_i^{k+1} = \begin{cases} 1, & \text{if } i \in \omega, \\ \frac{\rho^k}{\rho^k + \gamma}, & \text{otherwise.} \end{cases} \quad (27)$$

The solution procedure for  $g$  is organized as in Algorithm 1.

---

**Algorithm 1** Solving problem 18.

---

**Input:**  $\{X_i\}_{i=1}^m, \{P_i\}_{i=1}^m, \omega, \mathcal{M}, \mu, \lambda$ .

**Initialize:**  $u = y^k - \frac{c_1^k}{\rho^k} + \frac{\gamma}{\rho^k} P_\omega(z) - \frac{1}{\rho^k} t^k, v^0 = 0, k = 0$

**while**  $|f(v)| > 10^{-10}$  **do**

    Evaluate the function  $f(v^k)$  according to Eq.(25).

    Compute the gradient of  $f(v)$  at point  $v^k$  according to Eq.(26).

    Update  $v$  by  $v^{k+1} = v^k - \frac{f(v^k)}{\nabla f(v^k)}$

$k \leftarrow k + 1$

**end while**

**Output:**  $g$  via Eq.(24)

---

### 3.2.3 Updating $\mathcal{Y}^{k+1}$

By keeping all other variable fixed,  $\mathcal{Y}^{k+1}$  can be updated by solving the following optimization problem,

$$\min_{\mathcal{Y}} \quad \frac{\mu}{\rho^k} \|\mathcal{Y}\|_{\Phi, w, S_p}^p + \frac{1}{2} \left\| \mathcal{G}^{k+1} + \frac{\mathcal{C}^k}{\rho^k} - \mathcal{Y} \right\|_F^2. \quad (28)$$

To solve it, we first introduce the Theorems 1, which is proved in the Appendix A.1.

**Theorem 1.** Suppose  $\mathcal{A} \in \mathbb{R}^{n_1 \times n_2 \times n_3}$ ,  $l = \min(n_1, n_2)$ ,  $w_1 \geq w_2 \geq \dots \geq w_l \geq 0$ . Given the model

$$\min_{\mathcal{X}} \quad \tau \|\mathcal{X}\|_{\Phi, w, S_p}^p + \frac{1}{2} \|\mathcal{X} - \mathcal{A}\|_F^2, \quad (29)$$

then the optimal solution to the model (29) is

$$\mathcal{X}^* = (\text{fold}(\text{unfold}(\mathcal{S}_{\tau, w, p}(\mathcal{A}_\Phi)); \text{unfold}(\mathcal{A}_{\Phi^c})))_{\overline{\Phi}^\top}, \quad (30)$$

where  $\mathcal{S}_{\tau, w, p}(\mathcal{A}_\Phi)$  is a tensor, which the  $i$ -th frontal slice is  $\mathcal{S}_{\tau, w, p}(A_\Phi^{(i)})$ .

Therefore, the optimal solution of Eq.(28) is

$$\mathcal{Y}^{k+1} = \left( \text{fold} \left( \text{unfold} \left( \mathcal{S}_{\frac{\mu}{\rho^k}, w, p}(\mathcal{B}_\Phi^k) \right); \text{unfold}(\mathcal{B}_{\Phi^c}^k) \right) \right)_{\overline{\Phi}^\top}, \quad (31)$$

where  $\mathcal{B}^k = \mathcal{G}^{k+1} + \frac{\mathcal{C}^k}{\rho^k}$ ,  $\mathcal{S}_{\frac{\mu}{\rho^k}, w, p}(\mathcal{B}_\Phi^k)$  see the proof of the Theorem 1 in the Appendix A.1.

Based on the description above, the pseudo code is summarized in Algorithm 2.

---

**Algorithm 2** Solving problem (11)

---

**Input:**  $\{X_i\}_{i=1}^m, \{P_i\}_{i=1}^m, w, \mathcal{M}, \lambda, \mu, \gamma$ .  
**Initialize:**  $k = 0, \eta = 1.1, \rho^0 = 10^{-4}, \{\delta_i^0 = \frac{1}{m}\}_{i=1}^m, \mathcal{C}^0 = 0, \mathcal{G}^0 = \mathcal{Y}^0 = \mathcal{M}$ .  
**while** not converged **do**  
    Update  $A^{k+1}$  via Eq.(16)  
    Update  $W_i^{k+1}$  via  $(X_i P_i X_i^\top)^{-1} X_i P_i A^{k+1 \top}$  for all  $i$ .  
    Update  $\delta_i^{k+1}$  via definition for all  $i$ .  
    Update  $\mathcal{G}^{k+1}$  via Algorithm 1.  
    Update  $\mathcal{Y}^{k+1}$  via Eq.(31)  
    Update  $\mathcal{C}^{k+1}$  via  $\mathcal{C}^{k+1} = \mathcal{C}^k + \rho^k (\mathcal{G}^{k+1} - \mathcal{Y}^{k+1})$ .  
    Update  $\rho^{k+1}$  via  $\rho^{k+1} = \eta \rho^k$ .  
     $k \leftarrow k + 1$ .  
**end while**  
**Output:**  $A, \{W_i\}_{i=1}^m$

---

### 3.3 Convergence Analysis

We mainly analyze the convergence property of Algorithm 2 in this section. To prove the convergence of Algorithm 2, we first prove the bounded of sequences  $\{\mathcal{C}^k\}, \{\mathcal{Y}^k\}$  etc.. Lemma 2 is given first and is proved in the Appendix A.2. Then convergence is shown as in Theorem 2, which is proved in the Appendix A.3.

**Lemma 2.** *The sequence  $\{\mathcal{C}_1^k\}, \{\mathcal{Y}^k\}, \{A^k\}, \{\{W_i^k\}_{i=1}^m\}, \{\mathcal{G}^k\}$ , and the augmented Lagrangian function Eq.(14), which are generated by Algorithm 2, are bounded.*

**Theorem 2.** *The sequence  $\{\mathcal{G}^k\}$  and  $\{\mathcal{Y}^k\}$  generated by Algorithm satisfy*

1.  $\lim_{k \rightarrow \infty} \|\mathcal{G}^k - \mathcal{Y}^k\|_F = 0,$
2.  $\lim_{k \rightarrow \infty} \|\mathcal{G}^{k+1} - \mathcal{G}^k\|_F = 0,$
3.  $\lim_{k \rightarrow \infty} \|\mathcal{Y}^{k+1} - \mathcal{Y}^k\|_F = 0.$

## 4 Experiments and Analyses

### 4.1 Experimental Settings

**Datasets:** The four datasets used in the experiment are shown Table 4.1, and their details are described below.

1. *Handwritten Digit Database\**: This dataset contains ten categories, i.e., 1-10. Each category has 200 samples and a total of six views, i.e., pixel averages, Fourier coefficients, profile correlations, Zernike moment, Karhunen-love coefficient, and morphological. In this experiment, we only used the first five views.
2. *3 Sources†*: This dataset contains 948 stories from three online resources, BBC, Reuters, and Guardian. In this experiment a subset containing 169 stories were reported in all resources was used for comparison with other methods. These 169 stories were classified into six classes, which are business, entertainment, health, politics, sport, and technology.

---

\*<http://archive.ics.uci.edu/ml/datasets/Multiple+Features>

†<http://erdos.ucd.ie/datasets/3sources.html>

3. *BBC Sport*[53] This dataset contains 737 documents about sport news articles. These documents are described by 2-4 views and divided into 5 categories. In our experiments, we selected a subset containing 116 samples described by four views.
4. *Orl*<sup>‡</sup>: This is a very popular face dataset with 400 images of faces provided by 40 persons, each with 10 photos. Since Orl is a single-view dataset, we extracted LBP, GIST, and pyramid of the histogram of oriented gradients and combined them with pixel features to form a 4-views dataset.

Table 4.1: Description of the multi-view datasets

Dataset	Class	View	Samples	Features
Handwritten	10	5	2000	240/76/216/47/64
3 Sources	6	3	169	3560/3631/3036
BBC Sport	5	4	116	1991/2063/2113/2158
Orl	40	4	400	41/399/399/41

**Incomplete multi-view data construction:** For each of the above datasets, we randomly selected  $p\%$  ( $p \in \{90, 70, 50, 30\}$ ) samples to make them into incomplete samples, where the deletion of randomly selected instances generates the incomplete samples.

**Compared methods:** The following methods can deal with incomplete multi-view data to be used as baselines in this experiment.

1. BSV [54]: BSV performs  $k$ -means clustering and nearest neighbor classification on all views and reports the optimal clustering and classification results, where the missing instances are completed in the average instance of the corresponding view.
2. Concat [54]: Concatenating all views into one single view and exploiting  $k$ -means and nearest neighbor to obtain the final clustering and classification results, where the missing instances are also filled in the average instance like BSV.
3. DAIMC [20]: This method used two techniques for consistent representation of all views, namely matrix decomposition based on alignment of instance information and sparse regression based on basis matrices.
4. IMSC-AGL [4]: The method acquires consensus low-dimensional representation based on spectral clustering and constructed graphs from low-rank representation.
5. TCIMC [10]: This method obtains the complete graph by tensor recovery for each view, and differ from our method in the tensor norm.

Our method firstly obtains the low-dimensional representation  $A$  of all samples and then uses  $k$ -means on  $A$ . We preform  $k$ -means several times to get the average result since it is sensitive to the initial value. We use  $k$ -nearest-neighbor to construct a graph for each view, i.e.,

$$M_{i(k,l)} = \begin{cases} e^{-\frac{\|X_{i(k,:)} - X_{i(l,:)}\|_2^2}{2\sigma^2}}, & X_{i(k,:)} \in k\text{-NN}(X_{i(l,:)}), \\ 0, & \text{otherwise} \end{cases}, \quad (32)$$

where  $k = 10$ ,  $\sigma = 1$ . For the missing positions in the  $M_i$ , we fill them with 0. The  $p$ ,  $w$ , and  $\Phi$  in the tensor norm  $\|\cdot\|_{\Phi, w, S_p}$  are set 0.6, **1**, and discrete cosine transform, respectively.

**Evaluation metrics:** The clustering of the experiment in this paper uses three common metrics, i.e., clustering accuracy (ACC), normalized mutual information (NMI), and Purity.

<sup>‡</sup><http://cam-orl.co.uk/facedatabase.html>

## 4.2 Experimental Result

Table 4.2 shows the clustering results of the six methods on four datasets. We can draw the following conclusions from it.

1. Our method has the best results in most cases compared to the other five methods. In the clustering task, the proposed method is approximately 5% better than the second-best method on the Orl dataset. Inevitable, some data for which some measure is not optimal, e.g., the clustering task of Handwritten, 3Sources, and BBC Sport datasets.
2. IMSC\_AGL, TCIMC, and our method are graph-based methods. Table 4.2 shows that IMSC\_AGL, TCIMC, and our method have better clustering performance than DAIMC on all datasets. This indicates that graph tools can improve the clustering performance. Both TCIMC and our method are based on graph complementation and both are based on tensor recovery, the difference is that different tensor norm are used. The experiments show that our method has better performance in clustering than TCIMC in most datasets.
3. From the experimental result in Table 4.2, it can be seen that the clustering performance have a downward trend in most datasets overall with the increase of view missing rate. This phenomenon shows that it is difficult to learn a reasonable and effective consensus representation on a dataset with a high miss rate. Too many missing instances can result in insufficient consensus and complementarity among views. The experiments results on all datasets show that our proposed method has a greater advantage in the case of higher missing rate.

## 4.3 Analysis of the Parameter Sensitivity

This section analyzes the sensitive of three parameters  $\lambda$ ,  $\mu$ , and  $\gamma$  on Handwritten, 3Sources, BBC Sport, and Orl datasets. We first set up a candidate set for  $\lambda$  and  $\mu$ , i.e.  $\{1, 3, 5, 7, 9\}$  and  $\{10, 30, 50, 70, 90\}$ , then execute our proposed method for clustering with different combinations of two parameters ( $\lambda \& \mu$ ). Then we also execute proposed method for clustering with different  $\gamma$  on candidate set  $\{1e-2, 1e-1, 1, 1e1, 1e2, 1e3, 1e4, 1e5, 1e6\}$ . Fig.4.1 and Fig.4.2 show the clustering performance versus the scale parameter  $\lambda \& \mu$  and  $\gamma$  on the four datasets with a missing rate of 70% respectively. The experimental results show that our method is relatively stable for hyperparameters  $\lambda$ ,  $\mu$ , and  $\gamma$ , and the clustering performance is usually optimal for  $\lambda = 3$ ,  $\mu = 10$ , and  $\gamma = 100$ .

## 4.4 Convergence Analysis

In section 3.3, we show that Algorithm 2 is convergent. Then we use numerical experiments to verify the convergence of the proposed algorithm. We conducted experiments on Handwritten, 3 Sources, BBC Sport, and Orl datasets with a missing rate of 70%. Figure 4.3 shows the convergence of the algorithm and the clustering performance of the model as the number of iteration increases. It can be seen from Fig.4.3 that the optimization method provided by us has good convergence, in which  $\|\mathcal{G}^{k+1} - \mathcal{G}^k\|_F$ ,  $\|\mathcal{Y}^{k+1} - \mathcal{Y}^k\|_F$ , and  $\|\mathcal{G}^k - \mathcal{Y}^k\|_F$  can rapidly decline and tend to be 0 in all four datasets. The clustering results also stabilize with increasing number of iterations.

## 4.5 The Effect of the Parameter $r$

In this section, we investigate the effect of the parameter  $r$  on the experimental result. We let  $r$  be 10 to 100 percent of  $n_3$  for each experiment on Handwritten, 3 Sources, BBC Sport, and Orl datasets with a missing rate of 70%, i.e.,  $r \in \{n_3 \times 10\%, n_3 \times 20\%, \dots, n_3 \times 100\%\}$ . Figure 4.4 shows that the clustering performance of our method on the Handwritten and Orl datasets tends to decrease with increasing  $r/n_3$ . The proposed model performance does not change significantly with increasing  $r/n_3$  on the 3Sources

Table 4.2: Average and standard values of ACC (%), NMI(%), AND Purity(%) of seven methods over four datasets.

Datasets	Method\Rate	ACC					NMI					Purity				
		0.9	0.7	0.5	0.3	0.1	0.9	0.7	0.5	0.3	0.1	0.9	0.7	0.5	0.3	0.1
Handwritten	BSV	47.15±2.86	52.04±24.95	62.51±19.99	67.47±35.51	38.79±1.09	45.34±9.94	54.09±8.35	60.78±11.11	47.15±2.83	52.77±17.79	62.51±17.69	68.80±23.08	51.27±1.21	57.06±2.66	68.80±23.08
	Concat	39.96±3.37	44.37±10.75	48.95±2.88	53.12±5.01	32.91±1.51	37.91±4.83	43.27±1.73	49.02±1.12	40.65±1.71	46.22±4.08	51.27±1.21	57.06±2.66	51.27±1.21	57.06±2.66	57.06±2.66
	DAIMC	84.51±0.00	85.21±0.06	87.13±0.04	86.61±0.05	73.23±0.01	76.64±0.01	77.17±0.03	77.24±0.02	84.51±0.01	86.75±0.01	87.18±0.02	86.73±0.23	87.18±0.02	86.73±0.23	86.73±0.23
	IMSC-AGL	94.14±0.00	94.32±0.00	<b>95.40±0.00</b>	<b>96.04±0.00</b>	88.07±0.00	88.12±0.01	90.01±0.00	91.34±0.00	94.14±0.00	94.34±0.00	<b>95.40±0.00</b>	<b>96.04±0.00</b>	<b>95.40±0.00</b>	<b>96.04±0.00</b>	<b>96.04±0.00</b>
	TCIMV	86.79±0.98	86.35±1.26	85.90±0.36	85.15±1.01	88.95±1.34	89.77±0.54	89.8±2.36	89.58±0.95	88.01±1.32	88.40±0.01	88.40±0.66	88.10±1.32	88.40±0.66	88.10±1.32	88.10±1.32
	Our	<b>99.60±0.00</b>	<b>99.95±0.00</b>	86.08±0.63	86.95±0.00	<b>98.94±0.00</b>	<b>99.86±0.00</b>	<b>90.10±2.13</b>	<b>91.37±0.00</b>	<b>99.60±0.00</b>	<b>99.95±0.00</b>	<b>99.60±0.00</b>	<b>99.95±0.00</b>	88.58±0.62	89.00±0.00	89.00±0.00
3Sources	BSV	35.50±3.11	35.74±12.46	36.09±8.01	35.62±15.77	8.53±11.81	9.29±12.87	8.56±11.76	7.92±6.29	38.99±5.24	39.88±12.93	39.64±16.10	39.17±12.2	42.48±61.37	52.60±61.97	52.60±61.97
	Concat	37.33±6.96	38.04±30.50	40.35±47.45	46.39±35.41	7.96±14.37	11.36±69.01	13.87±75.81	22.97±98.79	39.40±18.61	42.48±61.37	45.32±74.47	52.60±61.97	45.32±74.47	67.57±0.06	67.57±0.06
	DAIMC	46.86±0.00	53.37±1.93	50.29±0.00	49.76±0.04	44.29±0.00	46.03±3.02	45.38±0.16	47.53±0.35	62.13±0.00	68.52±0.68	68.28±0.10	67.57±0.06	68.28±0.10	76.69±1.26	76.69±1.26
	IMSC-AGL	60.95±1.55	57.45±1.20	<b>65.62±5.94</b>	<b>68.11±2.83</b>	59.17±0.19	60.55±0.10	<b>57.89±6.65</b>	<b>61.18±0.86</b>	77.75±0.09	77.28±0.09	<b>76.56±6.08</b>	<b>76.69±1.26</b>	<b>76.56±6.08</b>	<b>76.69±1.26</b>	<b>76.69±1.26</b>
	TCIMV	68.64±0.00	69.23±0.00	56.80±0.00	69.82±0.00	63.85±0.00	54.34±0.02	52.50±0.00	57.98±0.00	79.23±0.00	75.14±0.00	72.19±0.00	<b>78.10±0.00</b>	72.19±0.00	<b>78.10±0.00</b>	<b>78.10±0.00</b>
	Our	<b>74.41±0.16</b>	<b>78.70±0.14</b>	59.76±0.06	59.16±0.08	<b>63.97±0.22</b>	<b>66.29±0.11</b>	52.47±1.14	60.20±0.20	<b>79.28±0.09</b>	<b>82.25±0.14</b>	70.41±0.06	74.56±0.00	70.41±0.06	74.56±0.00	74.56±0.00
BBC Sport	BSV	33.88±4.46	34.13±7.63	35.26±4.86	34.65±14.00	5.82±3.72	6.23±5.19	6.11±10.06	6.54±19.41	35.00±3.34	35.17±6.73	36.21±5.11	35.60±13.71	36.21±5.11	35.60±13.71	35.60±13.71
	Concat	33.36±4.79	34.91±21.35	33.62±3.30	37.58±61.13	5.81±2.24	6.27±7.76	5.37±5.26	11.01±63.76	34.65±2.61	36.55±19.19	35.29±4.03	39.14±55.19	35.29±4.03	39.14±55.19	39.14±55.19
	DAIMC	60.69±0.19	66.38±1.98	61.81±1.33	62.16±5.85	46.45±0.95	55.52±0.55	45.28±2.29	37.03±19.07	68.10±0.83	75.26±1.49	68.62±1.51	65.00±7.46	68.62±1.51	65.00±7.46	65.00±7.46
	IMSC-AGL	66.21±0.13	78.45±0.00	69.66±0.79	75.00±0.00	51.17±0.83	69.55±0.00	57.68±0.31	68.60±0.40	76.55±0.13	87.93±0.00	82.58±0.79	87.84±0.07	82.58±0.79	87.84±0.07	87.84±0.07
	TCIMV	81.03±0.00	81.62±0.00	79.31±0.00	<b>81.89±0.00</b>	78.20±0.00	<b>83.58±0.00</b>	71.07±0.00	<b>76.19±0.00</b>	91.03±0.00	93.82±0.00	88.79±0.00	90.21±0.00	93.82±0.00	90.21±0.00	90.21±0.00
	Our	<b>83.62±0.00</b>	<b>81.90±0.00</b>	<b>82.76±0.00</b>	80.17±0.00	<b>83.03±0.00</b>	79.91±0.00	<b>77.31±0.00</b>	74.50±0.00	<b>93.11±0.00</b>	<b>93.96±0.00</b>	<b>92.34±0.00</b>	<b>90.52±0.00</b>	<b>93.96±0.00</b>	<b>90.52±0.00</b>	<b>90.52±0.00</b>
Ohl	BSV	43.10±2.98	40.70±1.22	42.27±1.92	42.4±1.6	47.81±0.20	47.93±0.80	48.58±0.79	48.62±0.13	46.18±1.20	44.47±0.42	45.92±1.04	45.72±0.17	45.92±1.04	45.72±0.17	45.72±0.17
	Concat	16.08±0.88	15.29±2.23	10.87±2.88	21.50±135.6	24.28±2.91	24.77±5.56	29.04±9.52	35.14±178.1	34.65±2.61	36.55±19.19	35.29±4.03	39.14±55.19	35.29±4.03	39.14±55.19	39.14±55.19
	DAIMC	56.18±6.47	58.7±4.36	61.08±1.89	53.99±5.19	70.95±1.91	73.70±2.07	76.18±1.89	78.90±2.60	58.82±0.76	61.05±0.71	63.19±3.15	68.45±4.96	63.19±3.15	68.45±4.96	68.45±4.96
	IMSC-AGL	71.20±4.95	73.38±4.66	61.43±2.52	73.88±4.44	83.22±1.39	86.79±0.36	84.13±3.86	86.0±0.37	87.43±3.86	87.77±1.88	74.19±2.18	76.73±2.19	87.77±1.88	76.73±2.19	76.73±2.19
	TCIMV	86.50±1.06	84.95±0.85	85.45±0.54	84.00±2.04	91.06±0.09	92.04±0.07	92.27±0.17	91.24±0.11	87.40±0.09	88.35±0.68	87.35±0.17	86.60±0.11	88.35±0.68	86.60±0.11	86.60±0.11
	Our	<b>92.10±2.04</b>	<b>88.72±4.83</b>	<b>87.87±2.37</b>	<b>89.45±1.76</b>	<b>96.02±0.24</b>	<b>96.25±0.36</b>	<b>94.98±0.16</b>	<b>96.23±0.28</b>	<b>92.65±1.07</b>	<b>90.63±1.88</b>	<b>90.07±0.75</b>	<b>92.30±1.27</b>	<b>90.07±0.75</b>	<b>92.30±1.27</b>	<b>92.30±1.27</b>

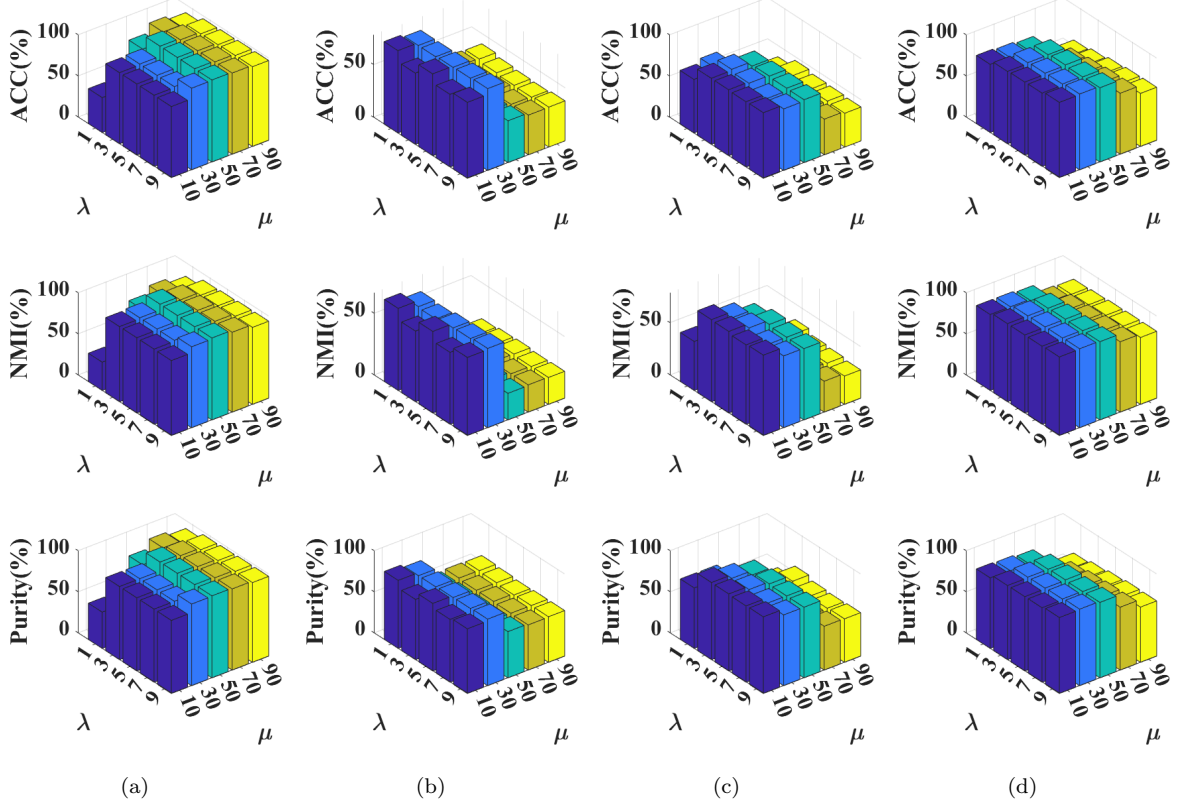


Figure 4.1: The clustering performance of parameters  $\lambda$  and  $\mu$  in different combination on (a) Handwritten, (b) 3Sources, (c) BBC Sport, and (d) Orl datasets with a missing rate of 70%.

and BBC Sport datasets. Figure 4.5 shows that the running time for solving  $\mathcal{Y}$  becomes larger as  $r/n_3$  increases on four datasets. In conclusion,  $r$  taking the value of  $n_3$  is not the optimal choice, so  $r < n_3$  is meaningful in this paper.

## 5 Conclusion

In this paper, we present an incomplete multi-view learning method, which uses the completed graphs obtained by tensor recovery to guide the data project into consistent low-dimensional subspace to preserve the geometry among samples. At the same time, we provide an optimization method based on inexact augmented Lagrange multiplier (ALM) and analyze its convergence and computational complexity. Finally, we verify the effectiveness of our proposed method on real datasets.

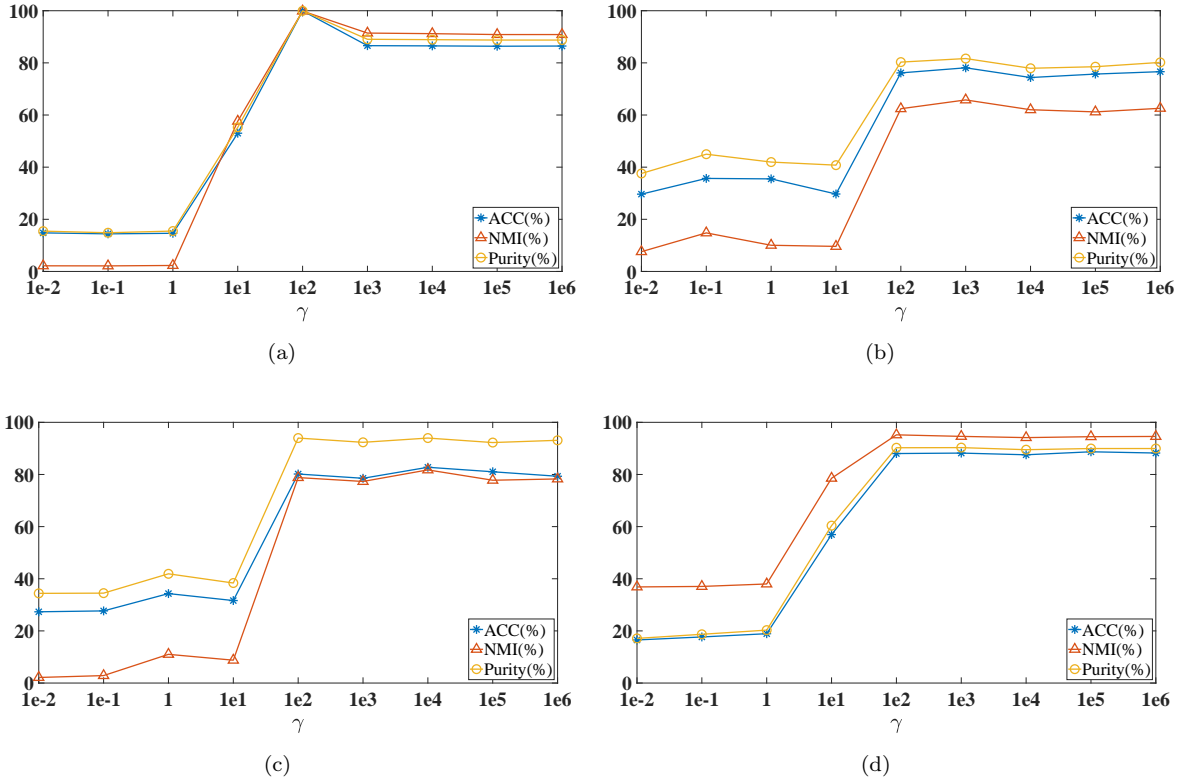


Figure 4.2: The clustering performance of parameter  $\gamma$  in different value on (a) Handwritten, (b) 3Sources, (c) BBC Sport, and (d) Orl datasets with a missing rate of 70%.



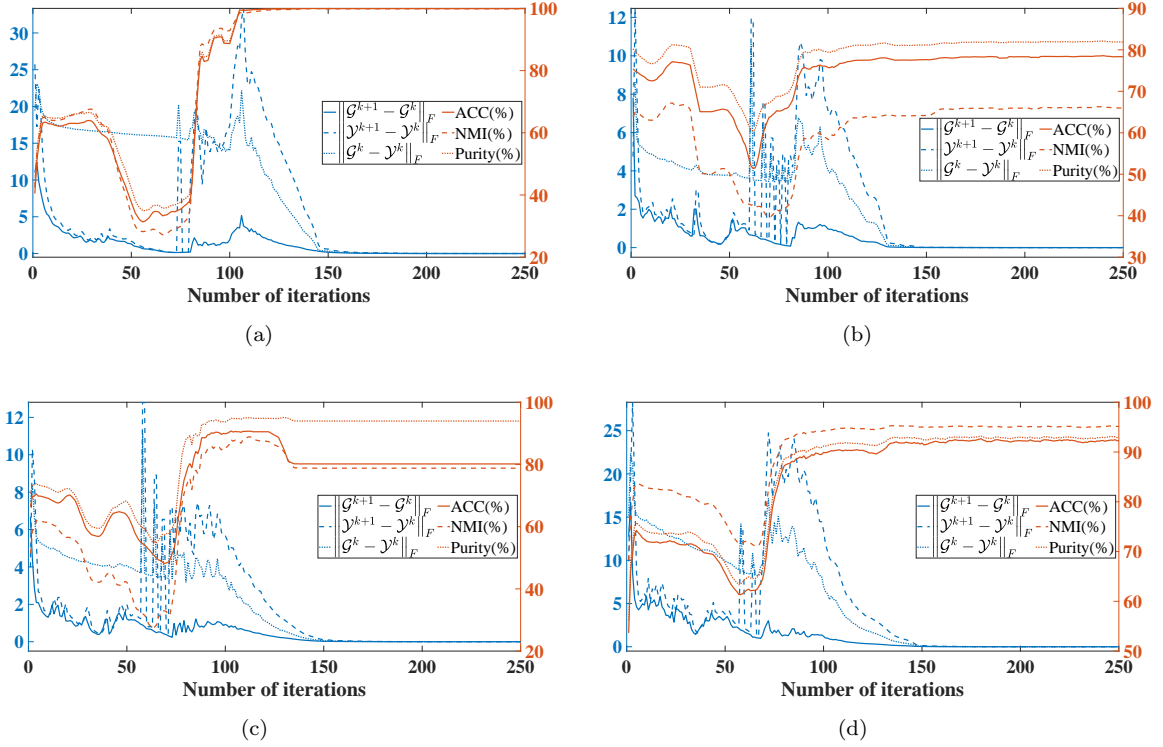
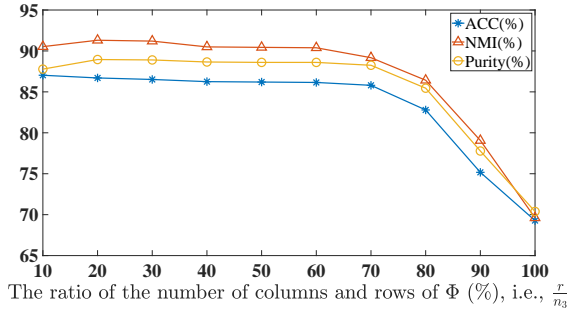
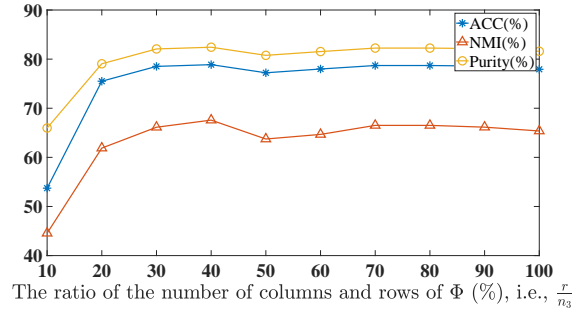


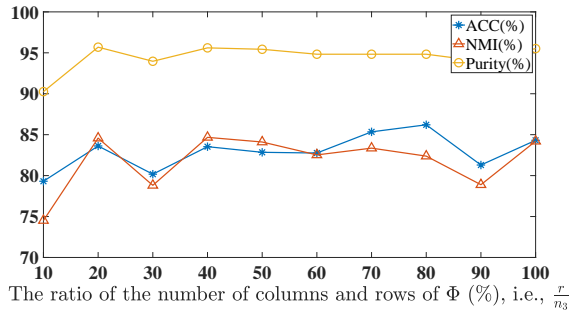
Figure 4.3: The convergence of the algorithm and the clustering performance of the model with the number of iterations on (a) Handwritten, (b) 3 Sources, (c) BBC Sport, (d) Orl datasets with a missing rate of 70%.



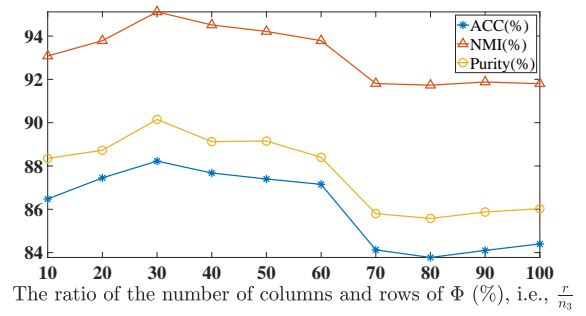
(a)



(b)



(c)



(d)

Figure 4.4: The clustering performance for different proportions of parameter  $r$  to  $n_3$  on the (a) Handwritten, (b) 3 Sources, (c) BBC Sport, and (d) Orl datasets with a missing rate of 70%.

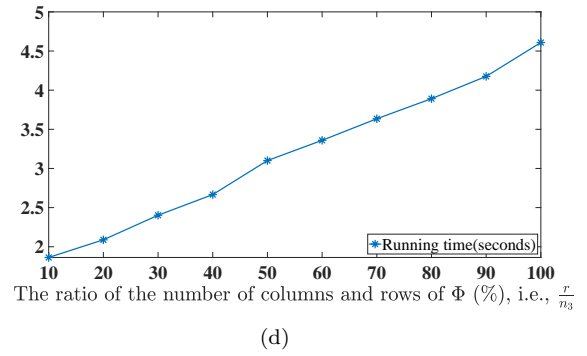
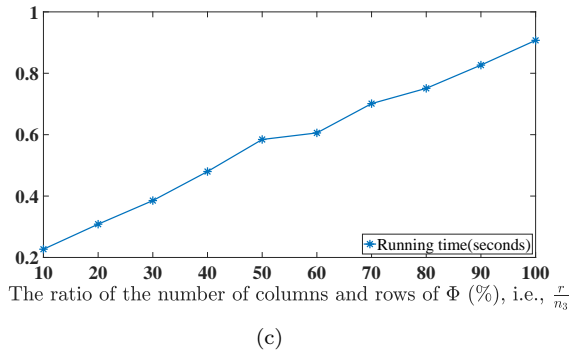
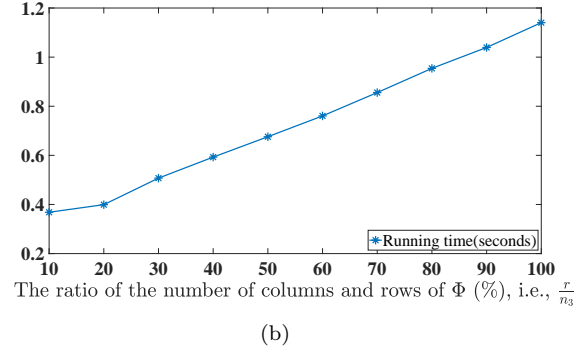
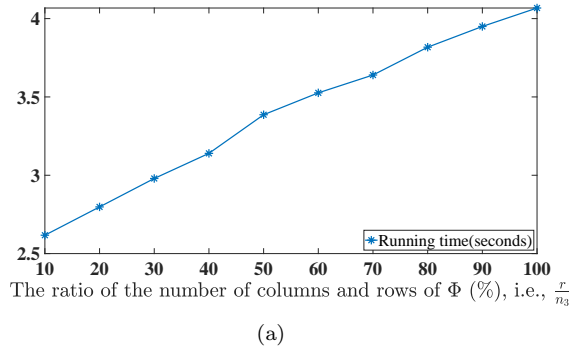


Figure 4.5: The running time for different proportions of parameter  $r$  to  $n_3$  on the (a) Handwritten, (b) 3 Sources, (c) BBC Sport, and (d) Orl datasets with a missing rate of 70%.

## A Appendix

### A.1 Proof of Theorem 1

Before proving Theorem 1, we first give Lemma 3 and Lemma 4.

**Lemma 3.** [55] *For the optimization problem*

$$\min_{x>0} \frac{1}{2} (x - \sigma)^2 + wx^p \quad (33)$$

with the given  $p$  and  $w$ , there is a specific threshold

$$\tau_p(w) = (2w(1-p))^{\frac{1}{2-p}} + wp(2w(1-p))^{\frac{p-1}{2-p}} \quad (34)$$

we have the following conclusion

1. When  $\sigma \leq \tau_p(w)$ , the optimal solution  $x_p(\sigma, w)$  of Eq.(33) is 0.
2. When  $\sigma > \tau_p(w)$ , the optimal solution is  $x_p(\sigma, w) = \text{sign}(\sigma) S_p(\sigma, w)$ , where  $S_p(\sigma, w)$  can be obtain by solving  $S_p(\sigma, w) - \sigma + wp(S_p(\sigma, w))^{p-1} = 0$ .

**Lemma 4.** [55] *Let  $Y = U_Y \Sigma_Y V_Y^\top$  be the SVD of  $Y \in \mathbb{R}^{m \times n}$ ,  $\tau > 0$ ,  $l = \min(m, n)$ ,  $w_1 \geq w_2 \geq \dots \geq w_l \geq 0$ , a global optimal solution of the following problem,*

$$\min_X \tau \|X\|_{w, S_p}^p + \frac{1}{2} \|X - Y\|_F^2, \quad (35)$$

is

$$S_{\tau, w, p}(Y) = U_Y P_{\tau, w, p}(Y) V_Y^\top \quad (36)$$

where  $P_{\tau, w, p}(Y) = \text{diag}(\gamma_1, \gamma_2, \dots, \gamma_l)$  and  $\gamma_i = x_p(\sigma_i(Y), \tau w_i)$  which can be obtained by Lemma 3.

The proof of the Theorem 1 is given as follows.

*Proof.* For a given semi-orthogonal matrix  $\Phi \in \mathbb{R}^{n_3 \times r}$ , there exists a semi-orthogonal matrix  $\Phi^c \in \mathbb{R}^{n_3 \times (n_3 - r)}$  satisfying  $\Phi^\top \Phi^c = I$ , where  $\Phi^c = [\Phi, \Phi^c] \in \mathbb{R}^{n_3 \times n_3}$ . According to definition, we have

$$\begin{aligned} \mathcal{X}^* &= \arg \min_{\mathcal{X}} \tau \|\mathcal{X}\|_{\Phi, w, S_p}^p + \frac{1}{2} \|\mathcal{X} - \mathcal{A}\|_F^2 \\ &= \arg \min_{\mathcal{X}} \tau \sum_{i=1}^r \left\| X_{\Phi}^{(i)} \right\|_{w, S_p}^p + \frac{1}{2} \|\mathcal{X}_{\Phi} - \mathcal{A}_{\Phi}\|_F^2 \\ &= \arg \min_{\mathcal{X}} \tau \sum_{i=1}^r \left\| X_{\Phi}^{(i)} \right\|_{w, S_p}^p + \frac{1}{2} \sum_{i=1}^r \left\| X_{\Phi}^{(i)} - A_{\Phi}^{(i)} \right\|_F^2 + \frac{1}{2} \sum_{j=1}^{n_3-r} \left\| X_{\Phi^c}^{(j)} - A_{\Phi^c}^{(j)} \right\|_F^2 \end{aligned} \quad (37)$$

In Eq.(37), each variable  $X_{\Phi}^{(i)}$  and  $X_{\Phi^c}^{(j)}$  is independent. Thus, it can be divided into  $n_3$  independent subproblem, i.e.,

$$\min_{\mathcal{X}} \tau \left\| X_{\Phi}^{(i)} \right\|_{w, S_p}^p + \frac{1}{2} \left\| X_{\Phi}^{(i)} - A_{\Phi}^{(i)} \right\|_F^2, \quad i = 1, 2, \dots, r \quad (38)$$

and

$$\min_{\mathcal{X}} \frac{1}{2} \left\| X_{\Phi^c}^{(j)} - A_{\Phi^c}^{(j)} \right\|_F^2, \quad j = 1, 2, \dots, n_3 - r \quad (39)$$

According to Lemma 4, the optimal solution of Eq.(38) and Eq.(39) are  $X_{\Phi}^{(i)*} = U_{A_{\Phi}^{(i)}} P_{\tau,w,p} \left( A_{\Phi}^{(i)} \right) V_{A_{\Phi}^{(i)}}^{\top}$  and  $X_{\Phi^c}^{(j)*} = A_{\Phi^c}^{(j)}$ , respectively. Therefore, we obtain optimal

$$\begin{aligned} \mathcal{X}_{\Phi}^* &= \text{fold} \left( X_{\Phi}^{(1)*}; X_{\Phi}^{(2)*}; \dots; X_{\Phi}^{(r)*}; X_{\Phi^c}^{(1)*}; X_{\Phi^c}^{(2)*}; \dots; X_{\Phi^c}^{(n_3-r)*} \right) \\ &= \text{fold} \left( S_{\tau,w,p} \left( A_{\Phi}^{(1)} \right); \dots; S_{\tau,w,p} \left( A_{\Phi}^{(r)} \right); A_{\Phi^c}^{(1)}; \dots; A_{\Phi^c}^{(n_3-r)} \right) \\ &= \text{fold} \left( \text{unfold} \left( S_{\tau,w,p} \left( \mathcal{A}_{\Phi} \right) \right); \text{unfold} \left( \mathcal{A}_{\Phi^c} \right) \right), \end{aligned} \quad (40)$$

then, further the optimal solution of Eq.(29) is  $\mathcal{X}^* = \left( \mathcal{X}_{\Phi}^* \right)_{\Phi}^{\top}$ .  $\square$

## A.2 Proof of Lemma 2

*Proof.* From the constraint on  $\mathcal{G}$  in Eq.(11), it is clear that  $\{\mathcal{G}^k\}$  must be bounded. Further according to Eq.(16) it is known that  $\{A^k\}$  and  $\{\{W_i^k\}_{i=1}^m\}$  are also bounded. In the  $k$ -th iteration in Algorithm 2, we have

$$\begin{aligned} \|\mathcal{C}^{k+1}\|_F &= \|\mathcal{C}^k + \rho^k (\mathcal{G}^{k+1} - \mathcal{Y}^{k+1})\|_F \\ &= \rho^k \left\| \mathcal{G}^{k+1} + \frac{\mathcal{C}^k}{\rho^k} - \mathcal{Y}^{k+1} \right\|_F \\ &= \rho^k \left\| \left( \mathcal{G}^{k+1} + \frac{\mathcal{C}^k}{\rho^k} - \mathcal{Y}^{k+1} \right)_{\bar{\Phi}} \right\|_F \\ &= \rho^k \left\| \mathcal{B}_{\bar{\Phi}}^k - \mathcal{Y}_{\bar{\Phi}}^{k+1} \right\|_F. \end{aligned} \quad (41)$$

From Eq.(31) we can get

$$\mathcal{Y}_{\bar{\Phi}}^{k+1} = \text{fold} \left( \text{unfold} \left( \mathcal{S}_{\rho^k, w, p} \left( \mathcal{B}_{\Phi}^k \right) \right); \text{unfold} \left( \mathcal{B}_{\Phi^c}^k \right) \right). \quad (42)$$

Substituting Eq.(42) into Wq.(41), we have

$$\begin{aligned} \|\mathcal{C}^{k+1}\|_F &= \rho^k \left\| \mathcal{B}_{\bar{\Phi}}^k - \text{fold} \left( \text{unfold} \left( \mathcal{S}_{\rho^k, w, p} \left( \mathcal{B}_{\Phi}^k \right) \right); \text{unfold} \left( \mathcal{B}_{\Phi^c}^k \right) \right) \right\|_F \\ &= \rho^k \left\| \mathcal{B}_{\bar{\Phi}}^k - \mathcal{S}_{\rho^k, w, p} \left( \mathcal{B}_{\Phi}^k \right) \right\|_F \\ &\leq \rho^k \sqrt{\sum_{i=1}^r \sum_{j=1}^{\min(n_1, n_2)} \left( \frac{J w_j \mu}{\rho^k} \right)^2} \\ &= \sqrt{\sum_{i=1}^r \sum_{j=1}^{\min(n_1, n_2)} (J w_j \mu)^2}, \end{aligned} \quad (43)$$

where  $J$  is the number of iterations in solving the problem (33). Thus,  $\{\mathcal{C}^k\}$  is bounded. Further according to Eq.(31) we can see that

$$\begin{aligned} \|\mathcal{Y}^{k+1}\|_F &= \left\| \text{fold} \left( \text{unfold} \left( \mathcal{S}_{\rho^k, w, p} \left( \mathcal{B}_{\Phi}^k \right) \right); \text{unfold} \left( \mathcal{B}_{\Phi^c}^k \right) \right) \right\|_F \\ &\leq \left\| \mathcal{S}_{\rho^k, w, p} \left( \mathcal{B}_{\Phi}^k \right) \right\|_F + \|\mathcal{B}_{\Phi^c}^k\|_F \\ &\leq \sum_{i=1}^r \left\| P_{\tau, w, p} \left( \mathcal{B}_{\Phi}^{(i)} \right) \right\|_F + \|\mathcal{B}_{\Phi^c}^k\|_F. \end{aligned} \quad (44)$$

It has already been mentioned that both  $\{\mathcal{C}^k\}$  and  $\{\mathcal{G}^k\}$  are bounded, so  $\{\mathcal{B}^k\}$  is bounded, and thus  $\{\mathcal{Y}^k\}$  is bounded.

The following proves that the augmented Lagrangian function Eq.(14) is bounded<sup>§</sup>. Let's first to prove

$$L_{\rho^k} \left( A^{k+1}, \{W_i^{k+1}\}_{i=1}^m, \mathcal{G}^k, \mathcal{Y}^k, \mathcal{C}^k \right) \leq L_{\rho^k} \left( A^k, \{W_i^k\}_{i=1}^m, \mathcal{G}^k, \mathcal{Y}^k, \mathcal{C}^k \right). \quad (45)$$

Recall Eq.(15), let  $f(A, W_i) = \left\| (A - W_i^\top X_i) P_i \right\|_F^2 + \lambda \operatorname{tr} (A L_{G_i^k} A^\top)$  and combining with  $\delta_i^k = n_i / \sqrt{f(A^k, W_i^k)}$ , we can derive

$$\sum_{i=1}^m \frac{n_i f(A^{k+1}, W_i^{k+1})}{2\sqrt{f(A^k, W_i^k)}} \leq \sum_{i=1}^m \frac{n_i f(A^k, W_i^k)}{2\sqrt{f(A^k, W_i^k)}}. \quad (46)$$

And since  $f(A, W_i) \geq 0$ , we have<sup>¶</sup>

$$\sum_{i=1}^m n_i \left( \sqrt{f(A^{k+1}, W_i^{k+1})} - \frac{f(A^{k+1}, W_i^{k+1})}{2\sqrt{f(A^k, W_i^k)}} \right) \leq \sum_{i=1}^m n_i \left( \sqrt{f(A^k, W_i^k)} - \frac{f(A^k, W_i^k)}{2\sqrt{f(A^k, W_i^k)}} \right). \quad (48)$$

Combining Eq.(46) and Eq.(48), we arrive at

$$\sum_{i=1}^m n_i \sqrt{f(A^{k+1}, W_i^{k+1})} \leq \sum_{i=1}^m n_i \sqrt{f(A^k, W_i^k)}. \quad (49)$$

Therefore, Eq.(45) is derived. In section 3.2.2 and section 3.2.3, since both  $\mathcal{G}$  and  $\mathcal{Y}$  subproblem have optimal solution, we have obviously

$$\begin{aligned} L_{\rho^k} \left( A^{k+1}, \{W_i^{k+1}\}_{i=1}^m, \mathcal{G}^{k+1}, \mathcal{Y}^{k+1}, \mathcal{C}^k \right) &\leq L_{\rho^k} \left( A^{k+1}, \{W_i^{k+1}\}_{i=1}^m, \mathcal{G}^k, \mathcal{Y}^k, \mathcal{C}^k \right) \\ &\leq L_{\rho^k} \left( A^k, \{W_i^k\}_{i=1}^m, \mathcal{G}^k, \mathcal{Y}^k, \mathcal{C}^k \right). \end{aligned} \quad (50)$$

Then

$$\begin{aligned} L_{\rho^k} \left( A^k, \{W_i^k\}_{i=1}^m, \mathcal{G}^k, \mathcal{Y}^k, \mathcal{C}^k \right) &= L_{\rho^{k-1}} \left( A^k, \{W_i^k\}_{i=1}^m, \mathcal{G}^k, \mathcal{Y}^k, \mathcal{C}^{k-1} \right) + \frac{\rho^k - \rho^{k-1}}{2} \|\mathcal{G}^k - \mathcal{Y}^k\|_F^2 \\ &\quad + \langle \mathcal{C}_1^k - \mathcal{C}_1^{k-1}, \mathcal{G}^k - \mathcal{Y}^k \rangle \\ &= L_{\rho^{k-1}} \left( A^k, \{W_i^k\}_{i=1}^m, \mathcal{G}^k, \mathcal{Y}^k, \mathcal{C}^{k-1} \right) \\ &\quad + \frac{\rho^k - \rho^{k-1}}{2} \left\| \frac{\mathcal{C}^k - \mathcal{C}^{k-1}}{\rho^{k-1}} \right\|_F^2 + \left\langle \mathcal{C}^k - \mathcal{C}^{k-1}, \frac{\mathcal{C}^k - \mathcal{C}^{k-1}}{\rho^{k-1}} \right\rangle \\ &= L_{\rho^{k-1}} \left( A^k, \{W_i^k\}_{i=1}^m, \mathcal{G}^k, \mathcal{Y}^k, \mathcal{C}^{k-1} \right) + \frac{\rho^k + \rho^{k-1}}{2\rho^{k-1}^2} \|\mathcal{C}^k - \mathcal{C}^{k-1}\|_F^2. \end{aligned} \quad (51)$$

---

<sup>§</sup>Note that one cannot state that Eq.(14) is bounded based on the fact that all variables are bounded due to  $\{\rho^k\}$  is unbounded

<sup>¶</sup>

**Corollary A.1.** For any positive number  $a$  and  $b$ , the following inequality holds

$$a - \frac{a^2}{2b} \leq b - \frac{b^2}{2b}. \quad (47)$$

Denote by  $b_c$  the bound of  $\|\mathcal{C}^k - \mathcal{C}^{k-1}\|_F^2$ , and combining Eq.(50) we have

$$L_{\rho^k} \left( A^{k+1}, \{W_i^{k+1}\}_{i=1}^m, \mathcal{G}^{k+1}, \mathcal{Y}^{k+1}, \mathcal{C}^k \right) \leq L_{\rho^0} \left( A^1, \{W_i^1\}_{i=1}^m, \mathcal{G}^1, \mathcal{Y}^1, \mathcal{C}^0, \right) + b_c \sum_{k=1}^{\infty} \frac{\rho^k + \rho^{k-1}}{2\rho^{k-1}^2}. \quad (52)$$

Since  $\rho > 1$ , the following inequality holds,

$$\sum_{k=1}^{\infty} \frac{\rho^k + \rho^{k-1}}{2\rho^{k-1}^2} \leq \sum_{k=1}^{\infty} \frac{\rho^k}{\rho^{k-1}^2} = \alpha \sum_{k=1}^{\infty} \frac{1}{\rho^{k-1}} < +\infty. \quad (53)$$

Combining Eq.(51), Eq.(52), and Eq.(53), it is known that the augmented Lagrangian function Eq.(14) is bounded.  $\square$

### A.3 Proof of Theorem 2

*Proof.* According to Lemma 2, we know  $\{\mathcal{C}^k\}$ ,  $\{\mathcal{G}^k\}$ , and  $\{\mathcal{Y}^k\}$  are all bounded. Bolzano-Weierstrass Theorem [56] shows that every bounded sequence of real numbers has a convergent subsequence. So there exists at least one accumulation point for  $\{\mathcal{C}^k\}$ ,  $\{\mathcal{G}^k\}$ , and  $\{\mathcal{Y}^k\}$ . Specifically, we can get

$$\lim_{k \rightarrow \infty} \|\mathcal{G}^k - \mathcal{Y}^k\|_F = \lim_{k \rightarrow \infty} \frac{1}{\rho^k} \|\mathcal{C}_1^k - \mathcal{C}_1^{k-1}\|_F = 0. \quad (54)$$

Similar to section 3.2.2, here again for each tube of  $\mathcal{G}^k$  is analyzed independently. Recalling that  $g^k$  is updated in the way Eq.(24), the following inequality holds,

$$\begin{aligned} \|g^{k+1} - g^k\|_F &= \left\| \frac{\rho^k}{\rho^k + \gamma} \max \left( P_w \left( u^k - \frac{1}{n} \mathbf{1} \mathbf{1}^\top u^k + \frac{1}{n} \mathbf{1} + v \mathbf{1} \right), 0 \right) \right. \\ &\quad \left. + \max \left( P_{w^c} \left( u^k - \frac{1}{n} \mathbf{1} \mathbf{1}^\top u^k + \frac{1}{n} \mathbf{1} + v \mathbf{1} \right), 0 \right) - g^k \right\|_F \\ &\leq \left\| \frac{\rho^k}{\rho^k + \gamma} \left( u^k - \frac{1}{n} \mathbf{1} \mathbf{1}^\top u^k + \frac{1}{n} \mathbf{1} + v \mathbf{1} - \frac{\rho^k + \gamma}{\rho^k} g^k \right) \right\|_F \\ &\quad + \left\| u^k - \frac{1}{n} \mathbf{1} \mathbf{1}^\top u^k + \frac{1}{n} \mathbf{1} + v \mathbf{1} - g^k \right\|_F. \end{aligned} \quad (55)$$

We analyze the first term and second term after the inequality sign of the Eq.(55) separately as follows,

$$\begin{aligned} &\left\| \frac{\rho^k}{\rho^k + \gamma} \left( u^k - \frac{1}{n} \mathbf{1} \mathbf{1}^\top u^k + \frac{1}{n} \mathbf{1} + v \mathbf{1} - \frac{\rho^k + \gamma}{\rho^k} g^k \right) \right\|_F \\ &= \left\| \frac{\rho^k}{\rho^k + \gamma} \left( y^k - \frac{c_1^k}{\rho^k} + \frac{\gamma}{\rho^k} P_w(m) - \frac{1}{\rho^k} t^k - \frac{1}{n} \mathbf{1} \mathbf{1}^\top \left( y^k - \frac{c_1^k}{\rho^k} + \frac{\gamma}{\rho^k} P_w(m) - \frac{1}{\rho^k} t^k \right) + \frac{1}{n} \mathbf{1} - g^k - \frac{\gamma}{\rho^k} g^k + v \mathbf{1} \right) \right\|_F \\ &= \left\| \frac{\rho^k}{\rho^k + \gamma} \left( \frac{c_1^{k-1} - 2c_1^k}{\rho^k} + \frac{\gamma}{\rho^k} P_w(m) - \frac{1}{\rho^k} t^k - \frac{1}{n} \mathbf{1} \mathbf{1}^\top \left( \frac{c_1^{k-1} - 2c_1^k}{\rho^k} + \frac{\gamma}{\rho^k} P_w(m) - \frac{1}{\rho^k} t^k \right) - \frac{\gamma}{\rho^k} g^k + v \mathbf{1} \right) \right\|_F, \end{aligned} \quad (56)$$

and

$$\begin{aligned} &\left\| u^k - \frac{1}{n} \mathbf{1} \mathbf{1}^\top u^k + \frac{1}{n} \mathbf{1} + v \mathbf{1} - g^k \right\|_F \\ &= \left\| y^k - \frac{c_1^k}{\rho^k} + \frac{\gamma}{\rho^k} P_w(m) - \frac{1}{\rho^k} t^k - \frac{1}{n} \mathbf{1} \mathbf{1}^\top \left( y^k - \frac{c_1^k}{\rho^k} + \frac{\gamma}{\rho^k} P_w(m) - \frac{1}{\rho^k} t^k \right) + \frac{1}{n} \mathbf{1} + v \mathbf{1} - g^k \right\|_F \\ &= \left\| \frac{c_1^{k-1} - c_1^k}{\rho^k} + \frac{\gamma}{\rho^k} P_w(m) - \frac{1}{\rho^k} t^k - \frac{1}{n} \mathbf{1} \mathbf{1}^\top \left( \frac{c_1^{k-1} - c_1^k}{\rho^k} + \frac{\gamma}{\rho^k} P_w(m) - \frac{1}{\rho^k} t^k \right) + v \mathbf{1} \right\|_F. \end{aligned} \quad (57)$$

The following shows that  $v$  tends to 0 when  $k$  tends to infinity. According to the definition of  $u^k$  the following equation holds,

$$\lim_{k \rightarrow \infty} \|u^k - g^k\|_2 = \left\| g^k + \frac{c_1^{k-1} - 2c_1^k}{\rho^k} + \frac{\gamma}{\rho^k} P_w(m) - \frac{1}{\rho^k} t^k - g^k \right\|_2 = 0. \quad (58)$$

Combining Eq.(24) and Eq.(25), Eq.(58) implies that  $f(0) = 0$  when  $k$  tends to infinity, i.e.  $v$  tends to 0. In summary,  $\lim_{k \rightarrow \infty} \|g^{k+1} - g^k\|_2 = 0$  and hence

$$\lim_{k \rightarrow \infty} \|\mathcal{G}^{k+1} - \mathcal{G}^k\|_F = 0. \quad (59)$$

The following inequality holds for  $\mathcal{Y}^k$ ,

$$\begin{aligned} \|\mathcal{Y}^{k+1} - \mathcal{Y}^k\|_F &= \|\mathcal{Y}^{k+1} - \mathcal{G}^{k+1} - \mathcal{Y}^k + \mathcal{G}^k + \mathcal{G}^{k+1} - \mathcal{G}^k\|_F \\ &\leq \|\mathcal{Y}^{k+1} - \mathcal{G}^{k+1}\| + \|\mathcal{Y}^k - \mathcal{G}^k\| + \|\mathcal{G}^{k+1} - \mathcal{G}^k\|_F. \end{aligned} \quad (60)$$

Combining Eq.(54) and Eq.(59), therefore, we have

$$\lim_{k \rightarrow \infty} \|\mathcal{Y}^{k+1} - \mathcal{Y}^k\|_F = 0. \quad (61)$$

□

## Acknowledgments

We would like to acknowledge the assistance of volunteers in putting together this example manuscript and supplement.

## References

- [1] J. Zhao, X. J. Xie, X. Xu, and S. L. Sun. Multi-view learning overview: Recent progress and new challenges. *Information Fusion*, 38:43–54, 2017.
- [2] Yanbei Liu, Lianxi Fan, Changqing Zhang, Tao Zhou, Zhitao Xiao, Lei Geng, and Dinggang Shen. Incomplete multi-modal representation learning for alzheimer’s disease diagnosis. *Medical Image Analysis*, 69:101953, 2021.
- [3] L. S. Qiao, L. M. Zhang, S. C. Chen, and D. G. Shen. Data-driven graph construction and graph learning: A review. *Neurocomputing*, 312:336–351, 2018.
- [4] J. Wen, Y. Xu, and H. Liu. Incomplete multiview spectral clustering with adaptive graph learning. *IEEE Transactions on Cybernetics*, 50(4):1418–1429, 2020.
- [5] J. Wen, Z. Zhang, Z. Zhang, L. K. Fei, and M. Wang. Generalized incomplete multiview clustering with flexible locality structure diffusion. *IEEE Transactions on Cybernetics*, 51(1):101–114, 2021.
- [6] Nan Zhang and Shiliang Sun. Incomplete multiview nonnegative representation learning with multiple graphs. *Pattern Recognition*, 123:108412, 2022.
- [7] J. Wen, K. Yan, Z. Zhang, Y. Xu, J. Q. Wang, L. K. Fei, and B. Zhang. Adaptive graph completion based incomplete multi-view clustering. *IEEE Transactions on Multimedia*, 23:2493–2504, 2021.



- [8] J. L. Liu, S. H. Teng, W. Zhang, X. Z. Fang, L. K. Fei, and Z. X. Zhang. Incomplete multi-view subspace clustering with low-rank tensor. In *IEEE International Conference on Acoustics, Speech and Signal Processing (ICASSP)*, pages 3180–3184, 2021.
- [9] J. Wen, Z. Zhang, Z. Zhang, L. Zhu, L. K. Fei, B. Zhang, and Y. Xu. Unified tensor framework for incomplete multi-view clustering and missing-view inferring. In *35th AAAI Conference on Artificial Intelligence / 33rd Conference on Innovative Applications of Artificial Intelligence / 11th Symposium on Educational Advances in Artificial Intelligence*, volume 35 of *AAAI Conference on Artificial Intelligence*, pages 10273–10281, 2021.
- [10] W. Xia, Q. X. Gao, Q. Q. Wang, and X. B. Gao. Tensor completion-based incomplete multiview clustering. *IEEE Transactions on Cybernetics*, 2022.
- [11] M. B. Blaschko, C. H. Lampert, and A. Gretton. Semi-supervised laplacian regularization of kernel canonical correlation analysis. In W. Daelemans, B. Goethals, and K. Morik, editors, *Machine Learning and Knowledge Discovery in Databases, Part I, Proceedings*, volume 52 of *Lecture Notes in Artificial Intelligence*, pages 133–145. Springer-Verlag Berlin, 2009.
- [12] X. H. Chen, S. C. Chen, H. Xue, and X. D. Zhou. A unified dimensionality reduction framework for semi-paired and semi-supervised multi-view data. *Pattern Recognition*, 45(5):2005–2018, 2012.
- [13] X. D. Zhou, X. H. Chen, and S. C. Chen. Neighborhood correlation analysis for semi-paired two-view data. *Neural Processing Letters*, 37(3):335–354, 2013.
- [14] Yuan Yun-Hao, Wu Zhaoqi, Li Yun, Qiang Jipeng, Gou Jianping, and Zhu Yi. Regularized multiset neighborhood correlation analysis for semi-paired multiview learning. *Neural Information Processing. 27th International Conference, ICONIP 2020. Proceedings. Lecture Notes in Computer Science (LNCS 12533)*, pages 616–625, 2020.
- [15] W. Q. Yang, Y. H. Shi, Y. Gao, L. Wang, and M. Yang. Incomplete-data oriented multiview dimension reduction via sparse low-rank representation. *IEEE Transactions on Neural Networks and Learning Systems*, 29(12):6276–6291, 2018.
- [16] C. M. Zhu, C. Chen, R. G. Zhou, L. Wei, and X. F. Zhang. A new multi-view learning machine with incomplete data. *Pattern Analysis and Applications*, 23(3):1085–1116, 2020.
- [17] S. Y. Li, Y. Jiang, and Z. H. Zhou. Partial multi-view clustering. In *28th AAAI Conference on Artificial Intelligence*, pages 1968–1974, 2014.
- [18] Chang Xu, Dacheng Tao, and Chao Xu. Multi-view learning with incomplete views. *IEEE Transactions on Image Processing*, 24(12):5812–5825, 2015.
- [19] J. Wen, Z. Zhang, Y. Xu, and Z. F. Zhong. Incomplete multi-view clustering via graph regularized matrix factorization. In *Computer Vision - ECCV 2018 Workshops, Pt Iv*, volume 11132, pages 593–608, 2018.
- [20] Menglei Hu and Songcan Chen. Doubly aligned incomplete multi-view clustering. In *International Joint Conference on Artificial Intelligence (IJCAI)*, page 2262–2268, 2019.
- [21] M. L. Hu and S. C. Chen. One-pass incomplete multi-view clustering. In *33rd AAAI Conference on Artificial Intelligence / 31st Innovative Applications of Artificial Intelligence Conference / 9th AAAI Symposium on Educational Advances in Artificial Intelligence*, pages 3838–3845, 2019.
- [22] Jianlun Liu, Shaohua Teng, Lunke Fei, Wei Zhang, Xiaozhao Fang, Zhuxiu Zhang, and Naiqi Wu. A novel consensus learning approach to incomplete multi-view clustering. *Pattern Recognition*, 115:107890, 2021.

- [23] X. W. Liu, X. Z. Zhu, M. M. Li, L. Wang, E. Zhu, T. L. Liu, M. Kloft, D. G. Shen, J. P. Yin, and W. Gao. Multiple kernel k-means with incomplete kernels. *IEEE Transactions on Pattern Analysis and Machine Intelligence*, 42(5):1191–1204, 2020.
- [24] J. Wen, H. J. Sun, L. K. Fei, J. X. Li, Z. Zhang, and B. Zhang. Consensus guided incomplete multi-view spectral clustering. *Neural Networks*, 133:207–219, 2021.
- [25] Wenzhang Zhuge, Tingjin Luo, Hong Tao, Chenping Hou, and Dongyun Yi. Multi-view spectral clustering with incomplete graphs. *IEEE Access*, 8:99820–99831, 2020.
- [26] Xinwang Liu, Xinzhong Zhu, Miaomiao Li, Lei Wang, Chang Tang, Jianping Yin, Dinggang Shen, Huaimin Wang, and Wen Gao. Late fusion incomplete multi-view clustering. *IEEE transactions on pattern analysis and machine intelligence*, 41(10):2410–2423, 2018.
- [27] X. Zheng, X. W. Liu, J. J. Chen, and E. Zhu. Adaptive partial graph learning and fusion for incomplete multi-view clustering. *International Journal of Intelligent Systems*, 37(1):991–1009, 2022.
- [28] Xiao Zheng, Xinwang Liu, Jiajia Chen, and En Zhu. Adaptive partial graph learning and fusion for incomplete multi-view clustering. *International Journal of Intelligent Systems*, 37(1):991–1009, 2022.
- [29] M. Y. Xie, Z. H. Ye, G. Pan, and X. L. Liu. Incomplete multi-view subspace clustering with adaptive instance-sample mapping and deep feature fusion. *Applied Intelligence*, 51(8):5584–5597, 2021.
- [30] L. Zhao, Z. K. Chen, Y. Yang, Z. J. Wang, and V. C. M. Leung. Incomplete multi-view clustering via deep semantic mapping. *Neurocomputing*, 275:1053–1062, 2018.
- [31] C. Q. Zhang, Z. B. Han, Y. J. Cui, H. Z. Fu, J. T. Zhou, and Q. H. Hu. Cpm-nets: Cross partial multi-view networks. In *33rd Conference on Neural Information Processing Systems (NeurIPS)*, volume 32 of *Advances in Neural Information Processing Systems*, 2019.
- [32] Q. Q. Wang, Z. M. Ding, Z. Q. Tao, Q. X. Gao, and Y. Fu. Partial multi-view clustering via consistent gan. In *18th IEEE International Conference on Data Mining Workshops (ICDMW)*, IEEE International Conference on Data Mining, pages 1290–1295, 2018.
- [33] C. Xu, H. M. Liu, Z. Y. Guan, X. N. Wu, J. L. Tan, and B. L. Ling. Adversarial incomplete multiview subspace clustering networks. *IEEE Transactions on Cybernetics*.
- [34] Ian Goodfellow, Jean Pouget-Abadie, Mehdi Mirza, Bing Xu, David Warde-Farley, Sherjil Ozair, Aaron Courville, and Yoshua Bengio. Generative adversarial nets. In *Advances in neural information processing systems*, volume 27.
- [35] Yijie Lin, Yuanbiao Gou, Zitao Liu, Boyun Li, Jiancheng Lv, and Xi Peng. Completer: Incomplete multi-view clustering via contrastive prediction. In *Proceedings of the IEEE/CVF Conference on Computer Vision and Pattern Recognition*, pages 11174–11183, 2021.
- [36] Bo Zhang, Jie Hao, Gang Ma, Jinpeng Yue, and Zhongzhi Shi. Semi-paired probabilistic canonical correlation analysis. In *International Conference on Intelligent Information Processing*, pages 1–10. Springer.
- [37] T. Matsuura, K. Saito, Y. Ushiku, and T. Harada. Generalized bayesian canonical correlation analysis with missing modalities. In *15th European Conference on Computer Vision (ECCV)*, volume 11134 of *Lecture Notes in Computer Science*, pages 641–656, 2019.
- [38] P. Li and S. C. Chen. Shared gaussian process latent variable model for incomplete multiview clustering. *IEEE Transactions on Cybernetics*, 50(1):61–73, 2020.

- [39] C. Kamada, A. Kanezaki, T. Harada, and Acm. Probabilistic semi-canonical correlation analysis. In *ACM International Conference on Multimedia (ACM Multimedia)*, pages 1131–1134, 2015.
- [40] C. Wang. Variational bayesian approach to canonical correlation analysis. *IEEE Transactions on Neural Networks*, 18(3):905–910, 2007.
- [41] A. Kimura, H. Kameoka, M. Sugiyama, T. Nakano, E. Maeda, H. Sakano, and K. Ishiguro. Semicca: efficient semi-supervised learning of canonical correlations. *Proceedings of the 2010 20th International Conference on Pattern Recognition (ICPR 2010)*, pages 2933–2936, 2010.
- [42] Y. Luo, D. C. Tao, K. Ramamohanarao, C. Xu, and Y. G. Wen. Tensor canonical correlation analysis for multi-view dimension reduction. *IEEE Transactions on Knowledge and Data Engineering*, 27(11):3111–3124, 2015.
- [43] Hok Shing Wong, Li Wang, Raymond Chan, and Tiejong Zeng. Deep tensor cca for multi-view learning. *IEEE Transactions on Big Data*, 2021.
- [44] M. M. Cheng, L. P. Jing, and M. K. Ng. Tensor-based low-dimensional representation learning for multi-view clustering. *IEEE Transactions on Image Processing*, 28(5):2399–2414, 2019.
- [45] C. Q. Zhang, H. Z. Fu, S. Liu, G. C. Liu, X. C. Cao, and Ieee. Low-rank tensor constrained multiview subspace clustering. In *IEEE International Conference on Computer Vision*, IEEE International Conference on Computer Vision, pages 1582–1590, 2015.
- [46] J. L. Wu, Z. C. Lin, and H. B. Zha. Essential tensor learning for multi-view spectral clustering. *IEEE Transactions on Image Processing*, 28(12):5910–5922, 2019.
- [47] Zhenwen Ren, Quansen Sun, and Dong Wei. Multiple kernel clustering with kernel k-means coupled graph tensor learning. In *Proceedings of the AAAI Conference on Artificial Intelligence*, volume 35, pages 9411–9418.
- [48] J.D. Carroll. Generalization of canonical correlation analysis to three or more sets of variables. In *Proceedings of the 76th Annual Convention of the American Psychological Association*, volume 3, page 227–228, 1968.
- [49] J. Chen, G. Wang, and G. B. Giannakis. Graph multiview canonical correlation analysis. *IEEE Transactions on Signal Processing*, 67(11):2826–2838, 2019.
- [50] Feiping Nie, Jing Li, Xuelong Li, et al. Self-weighted multiview clustering with multiple graphs. In *IJCAI*, pages 2564–2570, 2017.
- [51] Ky Fan. On a theorem of weyl concerning eigenvalues of linear transformations i. *Proceedings of the National Academy of Sciences*, 35(11):652–655, 1949.
- [52] Anne Marsden. Eigenvalues of the laplacian and their relationship to the connectedness of a graph. *University of Chicago, REU*, 2013.
- [53] Derek Greene and Pádraig Cunningham. Practical solutions to the problem of diagonal dominance in kernel document clustering. In *Proceedings of the 23rd international conference on Machine learning*, pages 377–384, 2006.
- [54] Handong Zhao, Hongfu Liu, and Yun Fu. Incomplete multi-modal visual data grouping. In *IJCAI*, pages 2392–2398.
- [55] Yuan Xie, Shuhang Gu, Yan Liu, Wangmeng Zuo, Wensheng Zhang, and Lei Zhang. Weighted schatten  $p$ -norm minimization for image denoising and background subtraction. *IEEE transactions on image processing*, 25(10):4842–4857, 2016.

- [56] JE Kimber Jr. Two extended bolzano-weierstrass theorems. *American Mathematical Monthly*, pages 1007–1012, 1965.